



Published in final edited form as:

Coord Chem Rev. 2019 January 15; 379: 65–81. doi:10.1016/j.ccr.2017.09.007.

Nanoscale Metal-Organic Frameworks for Phototherapy of Cancer

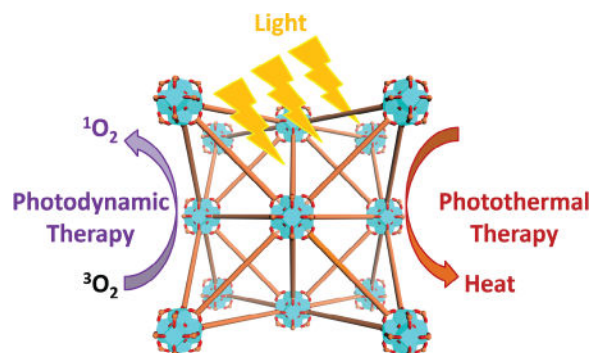
Guangxu Lan[‡], Kaiyuan Ni[‡], and Wenbin Lin^{*}

Department of Chemistry, University of Chicago, 929 East 57th Street, Chicago, Illinois 60637, United States

Abstract

Phototherapy involves the irradiation of tissues with light, and is commonly implemented in the forms of photodynamic therapy (PDT) and photothermal therapy (PTT). Photosensitizers (PSs) are often needed to improve the efficacy and selectivity of phototherapy *via* enhanced singlet oxygen generation in PDT and photothermal responses in PTT. In both cases, efficient and selective delivery of PSs to the diseased tissues is of paramount importance. Nanoscale metal-organic frameworks (nMOFs), a new class of hybrid materials built from metal connecting points and bridging ligands, have been examined as nanocarriers for drug delivery due to their compositional and structural tunability, highly porous structures, and good biocompatibility. This review summarizes recent advances on using nMOFs as nanoparticle PSs for applications in PDT and PTT.

Graphical abstract



Keywords

Metal-organic framework; Photodynamic therapy; Photothermal therapy; Nanophotosensitizers

Corresponding author at: Department of Chemistry, University of Chicago, 929 East 57th Street, Chicago, Illinois 60637, United States wenbinlin@uchicago.edu (W. Lin).

[‡]These authors contributed equally to this work.

Publisher's Disclaimer: This is a PDF file of an unedited manuscript that has been accepted for publication. As a service to our customers we are providing this early version of the manuscript. The manuscript will undergo copyediting, typesetting, and review of the resulting proof before it is published in its final citable form. Please note that during the production process errors may be discovered which could affect the content, and all legal disclaimers that apply to the journal pertain.

1. Introduction

Phototherapy dates back to ancient times [1, 2]. In 1903, Niels Ryberg Finsen was awarded the Nobel Prize in Physiology or Medicine for using short wavelength light to treat lupus vulgaris [3, 4], which was regarded as the beginning of modern phototherapy. Today, phototherapy is widely used to treat various diseases, such as atopic dermatitis [5], psoriasis [6], vitiligo [7], acne vulgaris [8, 9], and cancer [10]. However, due to the poor tissue penetration of light, pure phototherapy can only be used for superficial treatment. To enhance phototherapy, photosensitizers (PSs) are typically used to sensitize singlet oxygen generation in photodynamic therapy (PDT) and photothermal responses in photothermal therapy (PTT). Light of a specific wavelength is used to activate PSs to improve the therapeutic effects of PDT and PTT.

PDT treatment relies on three intrinsically nontoxic components: PSs, light, and tissue oxygen [11–14]. Irradiated by the light of an appropriate wavelength, a PS is promoted to the excited state, which reacts with nearby oxygen to generate reactive oxygen species (ROS), particularly singlet oxygen ($^1\text{O}_2$). By localizing both the PSs and the light exposure to tumor regions, PDT can selectively kill tumor cells while preserving surrounding normal tissues. As a result, PDT has been used to treat many different kinds of cancers, including esophageal cancer, non-small cell lung cancer, and head and neck cancer [14–18]. Porphyrin and its derivatives are the most commonly used PSs for PDT, and several of them, including PHOTOFRIN[®], VERTEPORFIN[®], FOSCAN[®], PHOTOCHLOR[®], and TALAPORFIN[®], have been approved for clinical use [16, 19, 20]. Despite their excellent photochemistry properties for ROS generation, these PSs have suboptimal tumor accumulation after systemic administration and tend to aggregate in solution due to their hydrophobicity, limiting the efficacy of PDT in the clinic [21]. Therefore, there is an ongoing need for effective delivery of PSs to tumors to improve the therapeutic effects of PDT.

In PTT, a PS is activated by light to the excited state, which then releases vibrational energy as heat to elevate local temperature above 40 °C to kill targeted cells. With moderate dark toxicity and light-activated cytotoxicity, PTT is also a local therapy with the ability to selectively damage tumors over normal tissues [22]. Because PTT treatment does not rely on local oxygen, it can be used to treat hypoxic cancers, which are typically non-responsive to PDT treatment. However, when normalized on the same energy of light irradiation, PTT is less effective than PDT due to lower cytotoxicity of the generated heat in comparison to the generated $^1\text{O}_2$ [23]. To further enhance the PTT efficacy, many powerful PSs, such as plasmonic gold nanorods [24] and phthalocyanin [25], have been developed. Selective delivery of PSs to tumor sites is also needed for more effective PTT treatment.

Nanoscience and nanotechnology have undergone rapid development over the past twenty years, with numerous types of nanomaterials now readily available. Nanoparticles (NPs) have provided a novel approach for enhanced cancer imaging and therapy due to their tunable sizes, modifiable surfaces, good biocompatibility, high agent loadings, and most importantly, the ability to preferentially deposit in tumors *via* the enhanced permeability and retention (EPR) effect [26–28]. The delivery of NPs to tumors can be further enhanced *via* active targeting of the receptors that are overexpressed on cancer cells [15, 29, 30].

Generally, nanomaterials can be broadly classified into three categories: (1) purely organic nanomaterials, such as micelles [31], liposomes [32], dendrimers [33], and polymeric hydrogel NPs [34]; (2) purely inorganic nanomaterials, such as metal NPs [24], metal oxide NPs [35], quantum dots [36], zeolites NPs [37], silica NPs [38], up-conversion NPs [39], and carbon nanomaterials [40]; (3) hybrid nanomaterials constructed *via* coordination bonds between inorganic and organic components, such as nanoscale metal-organic frameworks (nMOFs) and nanoscale coordination polymers (NCPs) [41–43].

MOFs are a new class of crystalline, porous hybrid materials constructed from metal-containing nodes, also known as secondary building units (SBUs), bridged by organic linkers. The archetype of MOFs dates back to Prussian blue (PB), a blue pigment with a cubic crystal structure constructed *via* Fe(II)-CN-Fe(III) coordination bonds [44]. MOFs have been intensely studied since the 1990s, and as a result of their tunability, nearly 20,000 MOFs with different structures have already been reported to date [43]. MOFs have been explored for diverse applications, including gas storage/separation [45–50], magnetism [51], nonlinear optics [52, 53], ferroelectricity [54], conductivity/semiconductivity [55–57], chemical sensing [58–62], catalysis [63–68], and energy conversion [69–71]. The Lin group pioneered in scaling down MOFs to the nanoscale and explored their potential in biomedical imaging [72–75] and drug delivery [41, 76–79]. In this review, we provide an overview on PDT and PTT and summarize recent advances in the applications of nMOFs in PDT and PTT of cancers.

2. PDT

PDT is an effective anticancer treatment that involves the administration of a tumor-localizing PS followed by light irradiation to generate highly cytotoxic ROS. Irradiated by light, a PS is first activated from the ground singlet state (S_0) to the excited singlet state (S_1). The PS at the S_1 state can undergo three different processes: decay to the ground state to generate fluorescence, vibrational relaxation to generate heat, or intersystem crossing to the triplet excited state (T_1) through a change in the electron spin orientation [80–82]. After intersystem crossing, the PS in the T_1 state can either decay to its ground state through emitting phosphorescence or exert PDT process by reacting with nearby triplet state molecules, particularly molecular oxygen (3O_2), *via* a Type-I process to generate radical species, including superoxide anions (O_2^-), or a Type-II process to generate 1O_2 [13, 14, 83, 84]. Most PDT treatments are believed to go through the Type-II process.

In a PDT treatment, a PS agent is first injected into the bloodstream of a patient, which is distributed throughout the whole body but is retained longer in cancer cells than in normal cells. The tumor site is then exposed to light 24 to 72 h after PS injection, when most of the PS agents have left normal tissues but significant amounts of them still remain in cancer cells. The PS agents accumulated in the tumors absorb the light and generate ROS, mainly 1O_2 , to destroy the cancer cells. Clinical studies have shown that PDT can treat certain types of cancers and pre-cancers, including head and neck cancer, mesothelioma, and pancreatic cancer. Compared to conventional chemotherapy and radiation therapy (RT), PDT has several advantages: (1) PDT is highly selective and less-invasive than surgery with little to no long-term side effects; (2) by localizing both the PSs and the light exposure to tumor

regions, PDT can be targeted very precisely to selectively kill tumor cells while preserving local tissues; (3) PDT treatment usually takes only a short time and can be repeated many times at the same site if needed with little or no scarring after the site heals; (4) PDT does not have cross resistance with other therapies, such as chemotherapy, RT, immunotherapy, and surgery; (5) PDT is most often performed on an outpatient basis and typically costs less than other cancer treatments.

Despite these advantages, PDT has not become a mainstream cancer therapy due to several severe drawbacks: (1) PDT cannot be used to treat large or deep-seated tumors because light cannot penetrate deeply (< 1 cm) through tissues; (2) As a local treatment, PDT cannot be used to treat cancers that have metastasized; (3) PSs used for PDT can leave patients very sensitive to light for a period of time, necessitating special precautions before and after PDT treatment. Significant efforts have been devoted to address these limitations of PDT over the past few decades, and many of these efforts were directed at improving two aspects of PDT: to discover or synthesize more powerful PSs and to improve the localization of PSs in tumors.

2.1 Optimization of PSs for PDT

PSs have been optimized to exhibit appropriate excitation wavelengths in order to increase tissue penetration for high PDT efficacy. The tissue penetration of light is wavelength dependent with the deepest tissue penetration at 800 nm. Generally, only PSs with the excitation wavelength located in the “tissue transparent” window of 650–800 nm, which have moderate tissue penetration of 3–10 mm, are regarded as having potential for clinical use [82, 85, 86]. In addition to this excitation wavelength requirement, there are several other guidelines for the design of clinically useful PSs: (1) the PS must have a strong absorption along with a high extinction coefficient (ϵ) in the “tissue transparent” window; (2) the PS must have no or minimal dark toxicity; (3) the PS must be chemically stable, photostable, and soluble or well dispersible in cellular environment; (4) the PS must be preferentially taken up and retained by tumor cells. Based on these design criteria, PSs have already evolved for three generations over the past few decades. Porphyrin-based PSs have been shown to be among the best PSs for PDT in the clinic.

Porphyrins refer to a series of heterocyclic macrocycles composed of four modified pyrrole subunits interconnected at their α carbon atoms *via* methylene bridges [86]. The aromatic porphyrin, with a total of 26 electrons in the conjugated system, has two groups of absorption bands: a sharp intense absorption band in the range of 390–425 nm, termed as the Soret band, and a set of relatively weak absorption bands in the range of 500–700 nm, termed as the Q-bands [87, 88]. Generally, in the case of porphyrin-based PSs, the last Q-band located in “tissue transparent” window is used to absorb light for PS excitation in PDT.

The first generation PSs were represented by clinically used Photofrin[®], which is also called Porfimer or hematoporphyrin Derivative (HpD). Hematoporphyrin (Hp) was discovered in 1841 and the investigation of HpD in the 1970s and early 1980s led to its clinical approval as Photofrin[®] for PDT in bladder cancer, esophageal cancer, and early non-small cell lung cancer [89–92]. The first generation PSs are non-ideal with relatively short wavelength

excitation at 630 nm, weak absorption at 630 nm, strong and persistent skin photosensitization, low tumor uptake, and relative poor tissue penetration.

Late 1980s witnessed the development of the second generation PSs represented by 5-aminolevulinic acid (ALA) and porphyrin derivatives, including chlorins, benzoporphyrins, phthalocyanines, and naphthalocyanines [13, 92, 93]. The second generation PSs feature near-infrared absorption, which affords deeper tissue penetration and extremely high absorption, with more than an order of magnitude higher molar ϵ 's than the first generation PSs. In addition, the second generation PSs alleviate skin photosensitization. However, the second generation PSs still suffer from suboptimal tumor accumulation and poor aqueous solubility or dispersity. Many of the second generation PSs require organic hydrotropes for administration in the clinical use, which can cause unwanted side effects. Nanotechnology has been used to deliver the third generation PSs, with the goal of improving tumor accumulation and eliminating organic hydrotropes.

2.2 Improving the localization of PSs in tumor

In order to selectively localize PSs in tumors and improve the solubility/dispersity of the second generation PSs, the third generation PSs emerged in 2000's by conjugating PSs with biologic components or delivering the PSs with nanocarriers [85, 94]. Two different strategies have been used to design the third generation PSs for the targeted delivery of PDT agents. The first strategy is to conjugate PSs to biological targeting molecules, including carbohydrate [95], proteins [96–98], peptides [99, 100], and antibodies [101], to realize active targeting of PSs. The second strategy is to encapsulate the PSs into porous nanocarriers, or to load the PSs on the surfaces of nanocarriers by physical absorption or covalent interactions, to realize passive targeting of PSs through the EPR effect [102, 103]. These nanocarriers can be broadly classified into two categories: organic nanomaterials such as liposomes [104–106] and dendrimers [107, 108], and inorganic nanomaterials such as gold NPs [109, 110] and silica NPs [111–113]. Meanwhile, the surfaces of these nanocarriers can be further modified with targeting molecules to actively target cancer cells. After accumulating in tumor cells, the PSs are slowly released from the nanocarriers and then irradiated by light to exert PDT effects.

Although the third generation PSs improve tumor accumulation and aqueous solubility/dispersity of PSs, they have their own limitations. First, when in close proximity, the excited states of PSs on the NPs will self-quench, leading to diminished PDT efficacy. Second, a large fraction of the generated ROS inside NPs cannot diffuse out of the NPs to reach intracellular targets for PDT effects, due to the short ROS diffusion length (20–220 nm for $^1\text{O}_2$ inside the cells). Third, the timing for light irradiation can be very difficult to optimize for NP-based PSs due to the necessity of balancing NP accumulation in tumors and the release of PSs from the NPs. As a result, no particle-based PSs have yet been approved for clinical use in spite of numerous efforts devoted to the development of the third generation PSs over the past decade.

To address the issues faced by NP PSs, the concept of nanophotosensitizers (nPSs) was proposed in 2011 to directly incorporate PSs into NPs as construction units rather than encapsulating PSs as cargoes [114, 115]. Compared to typical PSs delivery with NPs, nPSs

do not need to release PS molecules to exert PDT effects; instead, nPSs work as a whole PS to generate ROS, and the generated ROS can diffuse out of the matrix of the nPS to reach cellular or subcellular targets. Ideal nPS should simultaneously have high PS loadings without self-quenching, enhanced ROS generation efficiency over molecular PSs, and efficient diffusion of ROS from the nPS matrix to the cellular environment to cause cytotoxicity. Although some nPSs, such as porphyrin [114] and peptide self-assembled PSs [116–118], have been studied, no nPS met all of these requirements until the discovery of nMOF-based nPSs. We will discuss the design and applications of nMOFs as nPSs in PDT in the next section.

3. nMOFs for PDT

Constructed *via* coordination bonds between metal cluster secondary building units (SBUs) and bridging ligands, MOFs have emerged as a new class of hybrid materials with tunable, crystalline, and porous structures. These features make MOFs excellent candidates as nanocarriers for imaging contrast agents and therapeutic cargoes. Ideal sizes of nanocarriers should be larger than 10 nm to avoid rapid renal clearance, and smaller than 200 nm for efficient extravasation and optimum EPR effect [26–28]. Controlling the morphologies and sizes of MOF particles is a non-trivial task due to the intrinsic complexity of MOF compositions and typical MOF synthesis conditions. A number of factors are involved in MOF growth, including the concentrations and ratios of precursors (metal and organic linkers), the types and concentrations of modulators, solvents, temperature, water, and surfactant, making it difficult to predict and precisely control the morphologies and sizes of nMOFs. Through trials and errors, several synthetic methods, including solvothermal, surfactant-templated, and reverse microemulsion synthesis, have been demonstrated to be effective in nMOF synthesis [41]. The successful synthesis of these nMOFs provides the foundation for the rational design of nMOFs with desired structures, compositions, morphologies, and particle sizes in the future.

By judicious choices of functional SBUs or/and bridging ligands, a number of nMOFs have been designed and explored for biomedical imaging, including magnetic resonance imaging (MRI) [73, 74], computed tomography (CT) [119, 120], optical imaging [121] and sensing [122, 123], and drug delivery, including chemotherapeutic agents [124–126], PDT and PTT agents [127–154], nucleic acid [124, 155], and gas molecules such as nitric oxide [156–158]. Compared to purely organic and inorganic nanocarriers, nMOFs have several advantages: (1) high porosity of nMOFs permits a high payload of various diagnostic and therapeutic agents; (2) structural and compositional diversity of nMOFs allows for different sizes and morphologies, various chemical properties, and multiple functionalities; (3) biodegradability of nMOFs alleviates the concern of long-term toxicity.

Compositional and structural tunability of nMOFs has also allowed for the loading of imaging or/and therapeutic cargoes through several different methods: encapsulation into the nMOF channels, attachment to the ligands or the SBUs, or direct incorporation as nMOF linkers or metal nodes. The encapsulation method is the simplest and most frequently used, but premature cargo release can be a concern. Attachment to the linkers or metal nodes provides a nice option for postsynthetic loading if the attachment strength is appropriate to

balance the loading and release. The most unique feature of nMOFs in cargo delivery lies in the ability to directly incorporate the imaging or therapeutic agents into metal nodes or linkers, which is particularly important for designing nMOF PSs for PDT. The PSs can be derivatized to become organic linkers for the construction of nMOFs as nPSs. In the PDT process, the PSs do not need to be released from the matrix of nMOF to exert PDT effects. The nMOF nPSs can absorb light to generate ROS, which can rapidly diffuse out of nMOFs due to the highly porous structures.

As mentioned in the previous section, nMOFs are the most promising nPSs and have the potential of becoming the fourth generation PSs. Compared to other nPSs, the porous and crystalline structures of nMOFs isolate PSs from each other to avoid self-quenching of PS excited states. As a result, nMOFs can realize high PS loadings without suffering from self-quenching. Biodegradability of nMOFs alleviates long term toxicity whereas tunable compositions and structures allow for the optimization of nMOF nPSs for PDT applications. Since the first report on PDT with nMOFs in 2014 [127], at least 13 more papers on PDT of nMOFs have appeared in the literature [127–142, 159], highlighting tremendous interest in the use of nMOFs for PDT. Table 1 summarizes all of nMOFs that have been examined for PDT to date. We will discuss representative works in the following section.

3.1 The first nMOF for PDT

In 2014, the Lin group first reported a Hf-porphyrin nMOF, DBP-Hf, as a highly effective photosensitizer for PDT of resistant head and neck cancer [127]. DBP-Hf was constructed from Hf^{4+} and 5,15-di(P-benzoato)-porphyrin (H_2DBP) *via* a solvothermal method in dimethylformamide (DMF). DBP-Hf was first assigned as a typical UiO structure in the original paper based on its powder X-ray diffraction (PXRD) pattern, but was recently re-assigned as a new Hf-MOF structure with Hf_{12} cluster SBUs [160]. DBP-Hf displayed plate morphology of approximately 100 nm in diameter and 10 nm in thickness (Fig. 1a–b), which facilitates the diffusion of $^1\text{O}_2$ from the interior of DBP-Hf to the cell cytoplasm to exert cytotoxic effects. DBP-Hf carried exceptionally high PS loading of 77 wt% and processed 2.8 times better $^1\text{O}_2$ generation efficiency than H_2DBP according to the Singlet Oxygen Sensor Green (SOSG) assay (Fig. 1c). Comparing to H_2DBP , DBP-Hf not only overcame the aggregation issue of hydrophobic PSs, but also alleviated the self-quenching of PSs due to site isolation in the crystalline DBP-Hf structure. In addition, the highly porous structure of DBP-Hf facilitated the diffusion of generated $^1\text{O}_2$.

Consequently, DBP-Hf exhibited greatly enhanced PDT efficacy both *in vitro* and *in vivo*, when investigated in SQ20B head and neck cancer cells. By incubating SQ20B cells with DBP-Hf (30 $\mu\text{g}/\text{mL}$) for 4 hours, up to 30% DBP-Hf was taken up by the tumor cells to afford a high intracellular DBP-Hf concentration of ~ 1 mg/mL, which proved DBP-Hf could be effectively accumulated in tumor cells to achieve a high PS concentration. After incubation with free H_2DBP ligand and DBP-Hf at various concentrations, the cells were illuminated under 640 nm for 15 mins or 30 mins to investigate the cytotoxicity. Significant PDT efficacy was observed in the DBP-Hf treated group, while the H_2DBP treated group only showed moderate PDT efficacy (Fig. 1d). Meanwhile, no cytotoxicity was observed in dark control or blank control groups. DBP-Hf also exhibited significant *in vivo* efficacy, as

evidenced by complete tumor eradication in half of the mice receiving a single DBP-Hf dose (3.5 mg/kg, local administration) and a single light exposure (630 nm LED, 100 mW/cm² for 30 min) (Fig. 1e).

3.2 The first Chlorin-based nMOF for PDT

Despite the excellent performance in pilot animal studies, the photophysical properties of DBP-Hf are not optimal. DBP-Hf has the lowest energy absorption of 634 nm, which is near the high-energy edge of the tissue-penetrating window (600–900 nm), and a relatively small ϵ of 2200 M⁻¹·cm⁻¹. In molecular PS design, reduction of porphyrins to chlorins has been shown to shift the absorption to a longer wavelength with a concomitant increase in ϵ . Based on this rationale, Lin and co-workers designed the first chlorin-based nMOF, DBC-Hf, with much improved photophysical properties and PDT efficacy [128].

5,15-di(p-benzoato)chlorin (H₂DBC) was first synthesized by reduction of H₂DBP with toluenesulfonylhydrazide, and then treated with HfCl₄ and acetic acid in DMF at 80°C to afford a new nMOF, DBC-Hf. DBC-Hf had the lowest-energy Q band of 646 nm, which was red-shifted by 12 nm relative to DBP-Hf. In addition, DBC-Hf had a ϵ value of 24600 M⁻¹·cm⁻¹ for the lowest-energy Q band, which was 11-fold greater than that of DBP-Hf (Fig. 2b). DBC-Hf adopted the same plate morphology and topology structure as DBP-Hf as shown by transmission electron microscopy (TEM) images (Fig. 2a) and powder X-ray diffraction (PXRD) pattern. The plate diameters were 100–200 nm, while the thickness varied from 3.3 to 7.5 nm, which can further facilitate ROS diffusion during PDT compared to DBP-Hf (~10 nm in thickness). Consequently, DBC-Hf was approximately 3 times as efficient as DBP-Hf in generating ¹O₂ based on SOSG assay (Fig. 2c).

The superior PDT efficacy of DBC-Hf was demonstrated in two colorectal cancer mouse models, HT29 and CT26. DBC-Hf, DBP-Hf, or two PS ligands were intratumorally injected into mice at a ligand dose of 1 mg/kg. Upon light irradiation (650 nm LED, 100 mW/cm² for 15 min per fraction) for four times, only DBC-Hf effectively suppressed the tumor growth in both models. With higher ligand doses (3.5 mg/kg) and light irradiation (30 min per fraction), DBC-Hf successfully eradicated tumors in the HT29 model with a single treatment and in the CT26 model with two treatments (Fig. 2d–e). Interestingly, DBC-Hf-based PDT was discovered to induce both apoptosis and immunogenic cell death to contribute to the superior PDT efficacy.

3.3 Pegylated nMOF for PDT

In 2016, Liu and coworkers reported the Hf-TCPP nMOF (where TCPP is 5,10,15,20-tetrakis(4-carboxylphenyl)-porphyrin) of MOF-525 structure and demonstrated the ability to coat Hf-TCPP with polyethylene glycol (PEG) for efficient PDT efficacy upon intravenous injection [131]. Hf-TCPP was synthesized from Hf⁴⁺ and TCPP *via* a solvothermal method in DMF (Fig. 3a–b), displaying spherical morphology of approximately 130 nm in diameter based on DLS. PEG-grafted poly(maleicanhydride-*alt*-1-octadecene) (C₁₈PMH-PEG) was used to encapsulate hydrophobic Hf-TCPP to afford Hf-TCPP-PEG with good water dispersity. Hf-TCPP-PEG exhibited similar photophysical properties and ¹O₂ generation

efficacy as porphyrin nMOFs, such as DBP-Hf. Hf-TCPP-PEG also showed enhanced *in vitro* PDT efficacy against 4T1 cells.

To understand the *in vivo* behaviors of Hf-TCPP-PEG after intravenous injection, blood circulation, biodistribution, and clearance were studied in mice. After i.v. injection of Hf-TCPP-PEG in healthy Balb/c mice (Hf: 12.5 mg/Kg, TCPP: 24 mg/kg), blood was drawn from the mice at different time points to determine the Hf-TCPP-PEG concentration by quantifying the TCPP fluorescence. Hf-TCPP-PEG had a blood circulation half-life of ~ 3.27 h (Fig. 3c). Biodistribution and clearance of Hf-TCPP-PEG were investigated in 4T1 tumor-bearing mice by sacrificing the mice at different time points to determine the concentrations of Hf-TCPP-PEG in different organs. Hf-TCPP-PEG had a tumor accumulation of ~ 7% ID/g at 12 h post injection (Fig. 3d) with the majority of Hf⁴⁺ cleared in 7 days.

Hf-TCPP-PEG showed *in vivo* PDT therapeutic effect on 4T1 breast tumor model. 20 h post intravenous injection (Hf: 12.5 mg/Kg, TCPP: 24 mg/kg), the tumor sites of the mice were irradiated with laser (661 nm, 5 mW/cm²) for 1 h. In comparison to the control group, Hf-TCPP-PEG could partially suppress the tumor growth.

3.4 Targeted delivery of nMOF for *in vitro* PDT

Because ROS indiscriminately kills both diseased and normal cells, it is important to selectively accumulate the PSs in tumors to enhance the PDT efficacy. Zhou and coworkers modified the surface of Zr-based porphyrin nMOF, PCN-224, with folic acid (FA) to increase cell uptake of nMOFs and demonstrated higher *in vitro* PDT efficacy with FA-modified PCN-224 [134].

PCN-224 with a sphere morphology was constructed from a solvothermal reaction between Zr⁴⁺ and H₄TCPP in the presence of benzoic acid. By tuning the concentration of benzoic acid from 22 to 33 mg/mL in DMF, the size of PCN-224 NP increased from 24 to 232 nm (Fig. 4a). Size-dependent cytotoxicity assay was performed on human cervical cancer HeLa cells with PCN-224 particles of 30, 60, 90, 140, and 190 nm in diameter. After incubating HeLa cells with various sizes of PCN-224 in the concentration range of 0.5 to 40 μM based on TCPP for 12 h, 90 nm-PCN-224 showed the highest cell uptake. The *in vitro* PDT efficacy was tested for HeLa cells under irradiation at the 420 nm Soret band. At 20 μM concentration, 90 nm-PCN-224 gave the highest cytotoxicity of 81%, while 190 nm-PCN-224 gave the lowest efficacy of 49% (Fig. 4b).

90 nm-PCN-224 was then further modified with FA, a commonly used ligand for the folate receptor (FR) that is overexpressed in many tumor cells, by coordinating interaction between carboxylate end of FA and the Zr₆ SBUs. FA-PCN-224 showed slightly better cytotoxicity (~90%) than unmodified PCN-224 (~80%) on FR-positive HeLa cells (Fig. 4c), while similar cytotoxicity to unmodified PCN-224 was observed on FR-negative A549 cells. However, *in vivo* work is needed to confirm target-specific PDT of FA-PCN-224.

3.5 nMOFs for controlled singlet oxygen generation

Zhou and coworkers further reported on controlling the generation of $^1\text{O}_2$ using nMOFs built from photochromic molecules [130, 133]. Short-wavelength light was used to switch the photochromic molecule from the closed form to the open form to influence the ROS generation by nMOFs.

A Zn-TCPP-BPDTE MOF with a pillar-layer structure was synthesized from Zn^{2+} , TCPP, and 1,2-bis(2-methyl-5-(pyridine-4-yl)thiophen-3-yl)cyclopent-1-ene (BPDTE) *via* a solvothermal reaction in DMF. In the Zn-TCPP-BPDTE MOF, paddlewheel-type Zn cluster SBUs linked TCPP to form 2-D Zn-TCPP layers, which were connected by BPDTE *via* the Zn-N bonds to form a 3-D MOF. By taking advantage of the photochromic property of BPDTE, Zn-TCPP-BPDTE could adopt both open and closed forms. Upon UV irradiation at $\lambda=350$ nm, the open form of Zn-TCPP-BPDTE was transformed to the closed form, which could be reversibly transformed back to the closed form upon irradiation of visible light at $\lambda>450$ nm. Photophysical studies indicated that BPDTE in the open form of Zn-TCPP-BPDTE did not affect the $^1\text{O}_2$ generation of TCPP, while the BPDTE in the closed form of Zn-TCPP-BPDTE quenched the S_1 state of TCPP to reduce $^1\text{O}_2$ generation (Fig. 5).

The $^1\text{O}_2$ generation efficiencies of Zn-TCPP-BPDTE in the open and closed forms were evaluated by 1,3-diphenylisobenzofuran (DPBF), which can react with $^1\text{O}_2$ to decrease the absorption at 410 nm. Upon irradiation of 420 nm laser (6 mW/cm^2) for 60 seconds, Zn-TCPP-BPDTE in the closed form generated half as much $^1\text{O}_2$ as Zn-TCPP-BPDTE in the open form, suggesting the ability to modulate $^1\text{O}_2$ generation with switchable MOFs.

Zhou and coworkers used a similar strategy to control the $^1\text{O}_2$ generation by a UiO-66 nMOF doped with TCPP as the PS, and 1,2-bis(5-(4-carboxyphenyl)-2-methylthien-3-yl)cyclopent-1-ene (BCDTE) as the photochromic switch. In the cytotoxicity study, the doped UiO-66 with BCDTE in the open form exhibited a PDT cytotoxicity of ~90%, while the doped UiO-66 with BCDTE in closed form had a PDT cytotoxicity of only 10%. This result validated the strategy of incorporating both PSs and photochromic molecules into nMOFs to modulate $^1\text{O}_2$ generation and thus impact *in vitro* PDT efficacy.

3.6 BODIPY-containing nMOF for PDT

Diiodo-substituted BODIPYs (I_2 -BDPs), featuring high ϵ and low dark toxicities, are regarded as a potential PS in addition to porphyrin-based PSs. In 2016, Xie and coworkers reported the synthesis of a BODIPY-immobilized nMOF for PDT [135].

UiO-66 nMOF was first synthesized and then treated with monocarboxyl-modified I_2 -BDP (carboxy- I_2 -BDP) *via* solvent-assisted ligand exchange to afford the final product, UiO-PDT (Fig. 6a). The as-synthesized UiO-PDT maintained the UiO-66 structure based on the PXRD pattern, and the doping of I_2 -BDP was confirmed by ultraviolet–visible spectroscopy (UV-Vis), energy-dispersive X-ray spectroscopy (EDS) mapping, ^1H NMR, solid ^{13}C NMR, and inductively coupled plasma mass spectrometry (ICP-MS). These analyses indicated that 12.5 mol% of benzenedicarboxylate ligand was exchanged by carboxy- I_2 -BDP to afford a PS loading of 31.4 wt%. UiO-PDT processed similar octahedral morphology as UiO-66 with a mean diameter of 70 nm. Confocal laser scanning microscopy (CLSM) studies showed that

both UiO-PDT and carboxy-I₂-BDP could cross the cell membrane to accumulate in the cytoplasm, while flow cytometry studies indicated that UiO-PDT had 1.54 times higher cell uptake than carboxy-I₂-BDP. However, the ¹O₂ generation efficiency of UiO-PDT was lower than carboxy-I₂-BDP due to its heterogeneous nature (Fig. 6b). *In vitro* PDT efficacy of UiO-PDT and I₂-BDP was studied against B16F10, CT26, and C26 cell lines. Both UiO-PDT and I₂-BDP exhibited good cytotoxicity and inhibited cell growth by >80% in all three cell lines with light irradiation (80 mW/cm² for 10 min) (Fig. 6c). In spite of lower PDT efficacy of UiO-PDT than carboxy-I₂-BDP, this work provided a new approach to incorporate PDT agents into nMOFs and suggested the applicability of the solvent-assisted ligand exchange approach in loading other therapeutic cargoes onto nMOFs.

3.7 nMOF for combined PDT and immunotherapy

PDT is a local treatment and generally not effective in treating metastatic tumors. Based on their observation of immunogenic cell death caused by Hf-DBC, Lin and coworkers hypothesized that nMOF-mediated PDT could be combined with immune checkpoint blockade to treat metastatic tumors. They recently reported a novel treatment strategy that combined local PDT of a new chlorin-based nMOF, TBC-Hf, with checkpoint blockade immunotherapy to achieve effective and consistent abscopal responses in mouse models of colorectal cancers [129] (Fig. 7a).

TBC-Hf, constructed from a chlorin derivative, 5,10,15,20-tetra(p-benzoato)chlorin (H₄TBC) and Hf-based SBUs, was synthesized *via* a solvothermal reaction in DMF. TBC-Hf displayed a nanorod morphology of 50–100 nm in length and 30–60 nm in width based on TEM images. Based on PXRD pattern, TBC-Hf adopts the same structure as MOF-545 with a highly porous structure. TBC-Hf exhibited similar photophysical properties and ¹O₂ generation efficacy to DBC-Hf.

Checkpoint blockade immunotherapy, which uses small molecules or antibodies to stimulate the immunosuppressive microenvironment of tumors by modulating protein expressions and/or functions at dysregulated immune checkpoints, has emerged as a highly effective cancer treatment strategy. Indoleamine 2,3-dioxygenase (IDO), one such checkpoint, is often overexpressed in the tumor microenvironment. IDO causes tryptophan catabolism through the kynurenine pathway, facilitating the survival and growth of tumor cells by suppressing antitumor immune response. A small molecule IDO inhibitor (IDOi) was loaded into highly porous TBC-Hf to afford IDOi@TBC-Hf. The IDOi weight percentage after loading was determined to be 4.7% by thermogravimetric analysis (TGA) and ¹H NMR. Incubation in HBSS at 37 °C showed slow release of IDOi from IDOi@TBC-Hf, reaching 83.3% release after 24 h.

IDOi@TBC-Hf exhibited superior *in vivo* efficacy and abscopal effects in two colorectal mouse models, CT26 and MC38. Mice bearing a large primary tumor and a small distant tumor in the bilateral models were established for testing *in vivo* efficacy. Only the primary tumor was treated with a single injection of H₄TBC, H₄TBC+IDOi, TBC-Hf, or IDOi@TBC-Hf (TBC: 20 μmol/kg and IDOi: 1.5 mg/kg) and light irradiation (650 nm, 100 mW/cm² for 30 min). Mice treated with IDOi@TBC-Hf without light irradiation served as a dark control. At the endpoint, all the mice with primary tumors treated with IDOi@TBC-Hf

or TBC-Hf and PDT therapy had tumors only 1% size of PBS treated tumors in both models. H₄TBC with light irradiation and IDOi@TBC-Hf dark group failed to inhibit the tumor growth while H₄TBC plus IDOi with light irradiation slightly inhibited the tumor growth. Moreover, only IDOi@TBC-Hf with light irradiation group successfully reduced the sizes of the distant tumors, suggesting that the treatment evoked systemic antitumor immunity in mice. In comparison, TBC-Hf with light irradiation group and IDOi@TBC-Hf dark control only showed slight inhibition of distant tumor growth, showing ineffectiveness of monotherapies (Fig. 7b–e).

Mechanistic studies showed that TBC-Hf mediated PDT caused immunogenic cell death of cancer cells in the primary tumors, which activated innate immune system and promoted antigen presentation. The massive stressed and dying necrotic tumor cells in the PDT-treated primary tumor sites were engulfed by the innate immune effector cells followed by presenting tumor-derived antigenic peptides to T cells, thus stimulating a tumor-specific T cell response. Meanwhile, IDOi@TBC-Hf could both release IDOi into local tumor environment and enter blood circulation to systemically inhibit IDO activity to reverse the immunosuppressive tumor environments. PDT and IDOi checkpoint blockade therapy synergized with each other to kill local cancer cells and created an immunogenic tumor microenvironment systemically, leading to durable and consistent abscopal effects (Fig. 7a).

4. nMOFs for PTT

Thermal therapy, such as hypothermia and thermal ablation, is an emerging cancer treatment owing to its relatively simple operation, fast recovery, and short hospital stay [161]. Clinically, radiofrequency pulse, microwave radiation, and ultrasound wave have been employed as energy sources for thermal therapy of cancer. Mechanistically, local temperature elevated above 40 °C can damage cancerous tissue directly, and sensitize tumors to radiation or chemotherapy treatment.

PTT is a thermal therapeutic treatment induced by near-infrared light energy and has attracted attention in recent years. Different from PDT, PTT is an oxygen-independent and ROS-free process mediated by photothermal agents. After being excited by light of a specific wavelength, normally within the near-infrared (NIR) range, the activated PS falls back to its ground state and releases vibrational energy to generate heat. Such a non-radiative relaxation process converts light to local heat rapidly and can regress tumors by increasing the temperature in the tumor area sufficiently.

Light absorption and photothermal conversion efficiency together determine the performance of a PTT agent. In the past decade, there have been tremendous amounts of interest in developing NP PTT agents. Various inorganic and organic nanomaterials have been examined as PTT agents for treating cancer. Inorganic NP PTT agents include plasmonic gold nanostructures (nanospheres [162], nanoshells [163], nanorods [164], nanostars [165], and nanocages [166]), carbon (graphene [167], carbon nanotubes [168], and nanodiamonds [169]), iron oxide [170], palladium (Pd) nanosheets [171], metal chalcogenide [172], and polyoxometalate [173]. Several organic polymers, such as polypyrrole [174], polydopamine [175], and semiconducting polymer [176], have been

employed as surface coatings to increase blood circulation time and to reduce toxicity. With high light absorptivity and photothermal conversion efficiency, NP PTT agents can significantly increase local temperature in the tumor area compared to adjacent normal tissues, leading to anti-cancer efficacy with low side effects. Inspired by many potential biomedical applications of nMOFs, they are attracting significant attention as a platform to implement PTT and PTT-based combination therapies.

PTT as monotherapy typically cannot completely eradicate tumors due to inhomogeneous heat distribution in tumor tissues. Several strategies have been adopted to increase the anticancer efficacy of PTT and PTT-based combination therapies. First, better PTT agents with high light absorptivity in the NIR spectrum, high photothermal conversion efficiency, long blood circulation times, and enhanced tumor uptake are being sought to enhance photothermal therapy. Second, synergistic effects of PTT and other therapeutic modalities are being explored to enhance anticancer efficacy. Combination of PTT with ROS, small interference RNAs, or chemotherapeutics can drastically increase treatment efficacy. Third, image-guided PTT with theranostic agents based on multifunctional nanomaterials can also increase treatment efficacy of PTT *via* selective delivery of PTT agents to tumors.

With versatile tunability of nMOFs, the three strategies outlined above can be employed to design multifunctional nMOF hybrids for enhanced PTT. Both metal-cluster SBUs and bridging linkers can be functionalized to enhance photothermal conversion efficiency. Through post-synthetic modification or assembly from pre-modified linkers, functional moieties can be readily incorporated into nMOFs for combination therapies. Finally, encapsulation of functional components in nMOF cavities can further enhance the efficacy of PTT and PTT-based combination therapies. As summarized in Table 2, nMOFs have been used as PTT agents (nMOF-enabled PTT), as a platform for combining PTT with other diagnostic and therapeutic modalities (nMOF-combined PTT), and as hybrid nanomaterials for combined photodynamic therapy and photothermal therapy (nMOFs for PDT+PTT).

4.1 nMOF-enabled PTT

PB is mixed-valence hexacyanoferrate with a formula of $\text{Fe}^{\text{III}}_4[\text{Fe}^{\text{II}}(\text{CN})_6]_3 \cdot n\text{H}_2\text{O}$, and can be regarded as an archetypical MOF. Although devoid of large pores, PB exhibits high photothermal conversion efficiency, high photothermal stability, and good biocompatibility. PB was approved by US Food and Drug Administration (US FDA) for treating radionuclide exposure [177].

Yue and coworkers first reported PB NPs with PTT effects upon NIR light excitation [145]. Simple mixing of aqueous solutions of FeCl_3 and $\text{K}_4[\text{Fe}(\text{CN})_6]$ in the presence of citric acid as surfactant afforded PB nanocubes with controllable sizes from 10 to 50 nm. PB NPs absorbed broadly in the 500 nm to 900 nm range with the peak wavelength at 712 nm, due to the charge transfer transition between Fe(II) and Fe(III) centers [178]. PB NPs had a molar ϵ of $1.09 \times 10^9 \text{ M}^{-1} \text{ cm}^{-1}$ at 808 nm, comparable to that of gold nanorods ($5.24 \times 10^9 \text{ M}^{-1} \text{ cm}^{-1}$ at 808 nm). PB NPs showed much better photothermal stability than gold nanorods. With continuous exposure to an 808 nm laser, the temperature increase of a dispersion of gold nanorods gradually declined due to the melting of gold nanorods. Such a melting behavior

was not observed for PB NPs. The photothermal anti-cancer effect was further demonstrated by *in vitro* studies.

Chen and coworkers synthesized core-shell PB@MIL-100(Fe) nanocomposites for combined MRI and PTT [150]. PB@MIL-100(Fe) was shown to be a T_1 - T_2 dual-modal MRI contrast agent and could also be used for fluorescence optical imaging. More importantly, the PB core enabled PTT with NIR light irradiation. The as-prepared nanocomposite was also loaded with artemisinin at a loading of 848.4 mg/g. Both *in vivo* and *in vitro* data showed that artemisinin-loaded PB@MIL-100(Fe) possessed high antitumor efficacy by combining multi-modality imaging diagnosis, chemotherapy from triggered drug release, and NIR-activated PTT in a single system (Fig. 8).

Chen and coworkers further developed a nanopatform based on a PB analog, DOX@Mn₃[Co(CN)₆]₂@SiO₂@Ag (where DOX is doxorubicin), for combined chemotherapy and PTT [149]. The PB analog core endows T_1 - T_2 dual-modal MRI imaging due to paramagnetic Mn(II) and Co(II) ions. The Ag NPs deposited on the surface provided PTT capability. Loaded doxorubicin (DOX) could be released by local heat generated from Ag NP-enabled PTT. *In vitro* experiments indicated that combined PTT and chemotherapy treatment was superior to monotherapy. However, no *in vivo* experiments were performed.

Zhang and co-workers reported a similar PB@mSiO₂-PEG nanopatform with a high DOX loading [147]. The mesoporous silica and covalently conjugated PEG layer improved biocompatibility and photo-stability, while PB served both as a PTT agent and as a photoacoustic agent for theranostics. PB@mSiO₂-PEG with loaded DOX had good antitumor efficacy and diagnostic properties by integrating MRI, photoacoustic imaging (PAI), pH/light-triggered release, and combined PTT and chemotherapy.

Dai and coworkers designed and synthesized PB-coated gold NPs for simultaneous PAI, CT imaging, and PTT treatment of cancer [146]. With intravenous administration of PB-coated gold nanoparticles and one-dose treatment of NIR-laser irradiation of 900 J·cm⁻², mice bearing 100 mm³ tumors were completely cured without recurrence.

4.2 nMOF-combined PTT

Photothermal agents can be incorporated into nMOFs in several ways. The PTT agents can be encapsulated in the pores of nMOFs. Alternatively, photothermal nanomaterials can be presented as the core or the shell of a core-shell nMOF nanocomposite.

Wang and coworkers reported a Pd@Au/DOX@ZIF-8 nanocomposite for pH and NIR-triggered PTT-chemotherapy in 2017 [152]. Pd nanocubes were first synthesized as seeds and covered with Au nanosheets to afford Pd@Au NPs as a photothermal converter. Zeolitic imidazolate framework (ZIF)-8, an acid-degradable MOF, was used to encapsulate Pd@Au NPs and DOX to form the Pd@Au/DOX@ZIF-8 nanocomposite. Pd@Au/DOX@ZIF-8 converted 780 nm NIR light into heat to not only promote the release of DOX from ZIF-8 but also realize combined PTT-chemotherapy. The IC₅₀ value of DOX/Pd@Au@ZIF-8+NIR decreased more than twice compared to either Pd@Au@ZIF-8+NIR or DOX/

Pd@Au@ZIF-8 in *in vitro* cytotoxicity studies, indicating enhanced efficacy for combined PTT-chemotherapy treatment.

Tian and coworkers reported a simple one-pot synthesis of ZIF-8/graphene quantum dot NPs for combined PTT-chemotherapy in 2016 [148]. DOX was encapsulated into micropores of ZIF-8 *in situ* during hydrothermal MOF synthesis by taking advantage of weak coordinating interactions between DOX and zinc ions. The hydroxyl, epoxy, and carboxyl groups on graphene oxide (GO) quantum dots were utilized for the formation of MOF/GO nanocomposites *via* hydrogen bonding interaction with imidazolate ligands. The PTT effect of graphene quantum dots not only caused cancer cell death, but also enhanced drug release from ZIF-8.

Many NP PTT agents, such as gold nanorods, need to keep their morphologies during PTT treatment in order to maintain their PTT efficacy. This can sometimes be difficult to achieve due to thermally induced melting and aggregation of NP PTT agents. NP PTT agents were surface modified with silica shells or coated with PEG to stabilize them against thermally induced melting and aggregation. Fang *et al.* recently reported ZIF-8 coated gold nanorods for enhanced PTT with good stability and biocompatibility [144]. *In vitro* cytotoxicity studies showed that ZIF-coated gold nanorods had a lower dark toxicity ($IC_{50} = 157.19 \mu\text{g/mL}$) than uncoated gold nanorods ($IC_{50} = 23.26 \mu\text{g/mL}$). ZIF-8 coated gold nanorods showed higher PTT cytotoxicity ($IC_{50} = 4.45 \mu\text{g/mL}$) than uncoated gold nanorods ($IC_{50} = 7.39 \mu\text{g/mL}$). The ZIF-8 coating likely protected gold nanorods from melting.

Chen *et al.* developed a polypyrrole@MIL-100 core-shell nanocomposite for dual-modal imaging and combined PTT and chemotherapy [143]. The polypyrrole core served as a PTT agent and an organic PAI agent for deep tissue imaging. The MIL-100 shell was employed for DOX loading and MRI T_2 contrast imaging. It was proposed that Fe(III) ions mediated oxidative polymerization of pyrrole to form polypyrrole and subsequently binding of Fe(III) ions to the surface of polypyrrole facilitated the formation of MIL-100 shell on polypyrrole. The polypyrrole@MIL-100 core-shell nanocomposite enabled dual-modal imaging, light- and pH-triggered cargo release and combined PTT and chemotherapy treatment (Fig. 9).

4.3 nMOFs for combined PDT and PTT

nMOFs have also been explored as a versatile platform to combine PDT and PTT, two noninvasive light-induced anticancer treatments, to elicit synergistic effects and enhanced potency while reducing side effects. Yang and coworkers synthesized a therapeutic system based on a Au_{25} cluster-deposited MOF [137]. The as-synthesized $\text{Fe}_3\text{O}_4/\text{ZIF-8-Au}_{25}$ nanocomposites combined PDT-PTT therapy, magnetic targeting, and MRI imaging into one single system. PDT effect was caused by $^1\text{O}_2$ generated from Au_{25} clusters. Interestingly, the hyperthermia effect of magnetic Fe_3O_4 core was enhanced by PTT of Au_{25} clusters. In addition, Fe_3O_4 endowed magnetic targeting and MRI T_2 contrast imaging. A higher anti-tumor effect of PDT-PTT therapy with magnetic targeting was supported by *in vivo* experiments.

Yin and coworkers reported a porphyrin-based nMOF nanocomposite for dual-modality imaging-guided PDT-PTT combination therapy [138]. They utilized $\text{Fe}_3\text{O}_4@\text{C}$ as a core for

both T₂-weighted MRI imaging and photothermal therapy. The Fe₃O₄@C@Zr-TCPP nanocomposite was assembled in situ by treating Zr(IV) ion and H₄TCPP in the presence of Fe₃O₄@C. The PTT effect was adversely impacted by the Zr-TCPP shell, as shown in the laser-induced temperature increase data, but the photo-triggered anti-cancer potency was significantly increased in cytotoxicity tests. PDT and PTT in this system were induced by 655 nm and 808 nm lasers, respectively (Fig. 10).

5. Conclusions and perspectives

The exploration of nMOFs in biomedical imaging and anticancer drug delivery started more than 10 years ago [73, 77]. Potential applications of nMOFs in phototherapy were demonstrated only 5 years ago. A large number of papers have already appeared on phototherapy with nMOFs in the past 3 years, highlighting the strong interest in developing potentially clinically relevant phototherapy regimens based on nMOFs.

Since the first publication in 2014, nMOFs have already emerged as a promising nPS platform for PDT. Compared to other nPSs, nMOFs have several advantages for PDT: (1) by incorporating PSs as organic linkers, nMOFs achieve very high PS loadings while the crystalline structures of nMOFs avoid self-quenching of PSs by preventing them from aggregating; (2) highly porous structures of nMOFs not only facilitate the diffusion of oxygen and ROS, but also accommodate loading of diverse diagnostic and therapeutic agents for theranostics and synergistic therapy; (3) monocarboxylic modulators capping on the nMOFs can be easily replaced by other carboxyl modified functional molecules, such as PEG and targeting ligands, to endow biocompatibility and enhance tumor accumulation. With these beneficial features, nMOFs have great potential of becoming the fourth generation PSs.

Given synthetic tunability of nMOFs, we foresee many more efforts on designing new nMOFs for PDT. As PDT is a relatively well established treatment, future efforts should be focused on examining the utility of nMOF PSs under realistic *in vivo* conditions. With very little *in vivo* data available to date, it is too early to assess the clinical relevance of nMOFs in PDT.

Combing PDT with immunotherapy provides a powerful approach to treating metastatic cancers. As a local treatment, PDT can also produce a strong inflammatory response by inducing immunogenic cell death [14, 80, 94, 179]. The promising data from Lin's group on combining nMOF-enabled PDT and IDOi inhibition for treating metastatic cancer will inspire the exploration of this strategy using other nMOFs and checkpoint inhibitors. We expect significant amounts of research efforts in combining nMOF-mediated PDT and checkpoint blockade immunotherapy in the near future.

Compared to PDT, PTT monotherapy with nMOFs has not been explored in depth. Instead, by incorporating multiple functionalities into nMOF assemblies, researchers have explored combination therapies of PTT with other imaging and therapeutic modalities (such as MRI, fluorescence, PAI, radiotherapy, chemotherapy, and immune checkpoint blockade therapy) using nMOFs. Because the involvement of multiple therapies in these studies, it is difficult

to assess the contribution of PTT to the overall anticancer efficacy. The light dose for nMOF PTT studies are typically several times higher than the acceptable clinical dose of $\sim 180 \text{ J/cm}^2$. Several attempts have also been made to incorporate diagnostic/imaging functionalities into nMOFs with PTT capabilities, however, it is difficult to envision how such nMOF theranostics can be used in the clinic. Regulatory hurdles can also be significantly higher for nMOF assemblies with multiple components.

The synthetic tunability of nMOFs will allow fine-tuning of nMOFs for enhanced PDT and PTT efficacy. Judicious combination of nMOF phototherapy with other therapeutic modalities will likely further leverage the unique attributes of nMOFs and lead to superior antitumor efficacy. Although at their infancy, the future of nMOF-based phototherapy is bright. It is likely that nMOFs will find future applications in phototherapy or related therapeutic modalities for cancer treatment in the clinic.

Acknowledgments

We thank Dr. Kuangda Lu for his help. We acknowledge the National Cancer Institute (U01-CA198989) and the Ludwig Institute for Metastasis Research for funding support.

Abbreviations

PSs	photosensitizers
PDT	photodynamic therapy
PTT	photothermal therapy
MOFs	metal-organic frameworks
nMOFS	nanoscale metal-organic frameworks
ROS	reactive oxygen species
$^1\text{O}_2$	singlet oxygen
EPR	enhanced permeability and retention
NCPs	nanoscale coordination polymers
NPs	nanoparticles
SBU	secondary building units
S_0	ground singlet state
S_1	excited singlet state
T_1	excited triplet state
O_2^-	superoxide anions
Hp	hematoporphyrin

ALA	5-aminolevulinic acid
nPSs	nanophotosensitizers
MRI	magnetic resonance imaging
CT	computed tomography
H₂DBP	5,15-di(P-benzoato)-porphyrin
DMF	dimethylformamide
TEM	transmission electron microscopy
PXRD	powder X-ray diffraction
UiO	Universitetet i Oslo
SOSG	Singlet Oxygen Sensor Green
e	extinction coefficient
H₂DBC	5,15-di(p-benzoato)chlorin
H₄TBC	5,10,15,20-tetra(p-benzoato)chlorin
IDO	indoleamine 2,3-dioxygenase
IDOi	IDO inhibitor
TGA	thermogravimetric analysis
PEG	polyethylene glycol
C₁₈PMH-PEG	EG-grafted poly(maleicanhydride- <i>alt</i> -1-octdecene)
FA	folic acid
TCPP	5,10,15,20-Tetrakis(4-carboxylphenyl)-porphyrin
BPDTE	1,2-bis(2-methyl-5-(pyridine-4-yl)thiophen-3-yl)cyclopent-1-ene
DPBF	1,3-diphenylisobenzofuran
BCDTE	1,2-bis(5-(4-carboxyphenyl)-2-methylthien-3-yl)cyclopent-1-ene
BODIPYs	boron-dipyrromethene
I₂-BDP	diiodo-substituted BODIPYs
UV-Vis	ultraviolet-visible spectroscopy
EDS	energy-dispersive X-ray spectroscopy
ICP-MS	inductively coupled plasma mass spectrometry

CLSM	confocal laser scanning microscopy
NIR	near infra-red
PB	Prussian blue
US FDA	USA Food and Drug Administration
PAI	photoacoustic imaging
DOX	doxorubicin
ZIF	zeolitic imidazolate framework
GO	graphene oxide

References

- Ackroyd R, Kelty C, Brown N, Reed M. Photochemistry and Photobiology. 742001; :656–669. [PubMed: 11723793]
- Pushpan S, Venkatraman S, Anand V, Sankar J, Parmeswaran D, Ganesan S, Chandrashekar T. Current Medicinal Chemistry-Anti-Cancer Agents. 22002; :187–207. [PubMed: 12678743]
- Roelandts R. Journal of the American Academy of Dermatology. 462002; :926–930. [PubMed: 12063493]
- Møller KI, Kongshoj B, Philipsen PA, Thomsen VO, Wulf HC. Photodermatology, Photoimmunology & Photomedicine. 212005; :118–124.
- Patrizi A, Raone B, Ravaioli GM. Clinical, cosmetic and investigational dermatology. 82015; :511.
- Diffey B. Physics in Medicine and Biology. 251980; :405. [PubMed: 6996006]
- Adauwiyah J, Suraiya H. Med J Malaysia. 652010; :297–299. [PubMed: 21901949]
- Pei S, Inamadar AC, Adya KA, Tsoukas MM. Indian Dermatology Online Journal. 62015; :145. [PubMed: 26009707]
- Hession MT, Markova A, Graber EM. Dermatologic Surgery. 412015; :307–320. [PubMed: 25705949]
- Morton CA, Brown S, Collins S, Ibbotson S, Jenkinson H, Kurwa H, Langmack K, McKenna K, Moseley H, Pearse A. British Journal of Dermatology. 1462002; :552–567. [PubMed: 11966684]
- Juarranz Á, Jaén P, Sanz-Rodríguez F, Cuevas J, González S. Clinical and Translational Oncology. 102008; :148–154. [PubMed: 18321817]
- Henderson BW, Dougherty TJ. Photochemistry and Photobiology. 551992; :145–157. [PubMed: 1603846]
- Sharman WM, Allen CM, Van Lier JE. Drug Discovery Today. 41999; :507–517. [PubMed: 10529768]
- Agostinis P, Berg K, Cengel KA, Foster TH, Girotti AW, Gollnick SO, Hahn SM, Hamblin MR, Juzeniene A, Kessel D. CA: a cancer journal for clinicians. 612011; :250–281. [PubMed: 21617154]
- Master A, Livingston M, Gupta AS. Journal of Controlled Release. 1682013; :88–102. [PubMed: 23474028]
- Dolmans DE, Fukumura D, Jain RK. Nature Reviews Cancer. 32003; :380–387. [PubMed: 12724736]
- Lou P-J, Jones L, Hopper C. Technology in Cancer Research & Treatment. 22003; :311–317. [PubMed: 12892513]
- Bredell MG, Besic E, Maake C, Walt H. Journal of Photochemistry and Photobiology B: Biology. 1012010; :185–190.
- Bhaumik J, Mittal AK, Banerjee A, Chisti Y, Banerjee UC. Nano Research. 82015; :1373–1394.

20. Dhaneshwar S, Patil K, Bulbule M, Kinjawadekar V, Joshi D, Joshi V. International Journal of Pharmaceutical Sciences Review Research. 272014; :125–141.
21. Chouikrat R, Seve A, Vanderesse R, Benachour H, Barberi-Heyob M, Richeter S, Raehm L, Durand J-O, Verelst M, Frochot C. Current Medicinal Chemistry. 192012; :781–792. [PubMed: 22214454]
22. Doane TL, Burda C. Chemical Society Reviews. 412012; :2885–2911. [PubMed: 22286540]
23. Shanmugam V, Selvakumar S, Yeh C-S. Chemical Society Reviews. 432014; :6254–6287. [PubMed: 24811160]
24. Huang X, El-Sayed IH, Qian W, El-Sayed MA. Journal of the American Chemical Society. 1282006; :2115–2120. [PubMed: 16464114]
25. Peng J, Zhao L, Zhu X, Sun Y, Feng W, Gao Y, Wang L, Li F. Biomaterials. 342013; :7905–7912. [PubMed: 23891514]
26. Maeda H, Wu J, Sawa T, Matsumura Y, Hori K. Journal of Controlled Release. 652000; :271–284. [PubMed: 10699287]
27. Prabhakar U, Maeda H, Jain RK, Sevick-Muraca EM, Zamboni W, Farokhzad OC, Barry ST, Gabizon A, Grodzinski P, Blakey DC. American Association for Cancer Research. 732013; :2412–2417.
28. Albanese A, Tang PS, Chan WC. Annual Review of Biomedical Engineering. 142012; :1–16.
29. Petros RA, DeSimone JM. Nature Reviews Drug Discovery. 92010; :615–627. [PubMed: 20616808]
30. Bardhan R, Lal S, Joshi A, Halas NJ. Accounts of Chemical Research. 442011; :936–946. [PubMed: 21612199]
31. Kataoka K, Harada A, Nagasaki Y. Advanced Drug Delivery Reviews. 472001; :113–131. [PubMed: 11251249]
32. Torchilin VP. Nature Reviews Drug Discovery. 42005; :145–160. [PubMed: 15688077]
33. Lee CC, MacKay JA, Fréchet JM, Szoka FC. Nature Biotechnology. 232005; :1517–1526.
34. Hamidi M, Azadi A, Rafiei P. Advanced Drug Delivery Reviews. 602008; :1638–1649. [PubMed: 18840488]
35. Gupta AK, Gupta M. Biomaterials. 262005; :3995–4021. [PubMed: 15626447]
36. Gao X, Cui Y, Levenson RM, Chung LW, Nie S. Nature Biotechnology. 222004; :969.
37. Li Z, Hüve J, Krampe C, Luppi G, Tsotsalas M, Klingauf J, De Cola L, Riehemann K. Small. 92013; :1809–1820. [PubMed: 23335435]
38. Li Z, Barnes JC, Bosoy A, Stoddart JF, Zink JI. Chemical Society Reviews. 412012; :2590–2605. [PubMed: 22216418]
39. Shen J, Zhao L, Han G. Advanced Drug Delivery Reviews. 652013; :744–755. [PubMed: 22626980]
40. Bianco A, Kostarelos K, Partidos CD, Prato M. Chemical Communications. 2005; :571–577. [PubMed: 15672140]
41. He C, Liu D, Lin W. Chemical Reviews. 1152015; :11079–11108. [PubMed: 26312730]
42. Giménez-Marqués M, Hidalgo T, Serre C, Horcajada P. Coordination Chemistry Reviews. 3072016; :342–360.
43. Lismont M, Dreesen L, Wuttke S. Advanced Functional Materials. 272017;
44. Itaya K, Uchida I, Neff VD. Accounts of Chemical Research. 191986; :162–168.
45. Eddaoudi M, Kim J, Rosi N, Vodak D, Wachter J, O'keeffe M, Yaghi OM. Science. 2952002; :469–472. [PubMed: 11799235]
46. Murray LJ, Dinc M, Long JR. Chemical Society Reviews. 382009; :1294–1314. [PubMed: 19384439]
47. Suh MP, Park HJ, Prasad TK, Lim D-W. Chemical Reviews. 1122011; :782–835. [PubMed: 22191516]
48. Li J-R, Sculley J, Zhou H-C. Chemical Reviews. 1122011; :869–932. [PubMed: 21978134]
49. Sumida K, Rogow DL, Mason JA, McDonald TM, Bloch ED, Herm ZR, Bae T-H, Long JR. Chemical Reviews. 1122011; :724–781. [PubMed: 22204561]

50. He Y, Zhou W, Qian G, Chen B. *Chemical Society Reviews*. 432014; :5657–5678. [PubMed: 24658531]
51. Kurmoo M. *Chemical Society Reviews*. 382009; :1353–1379. [PubMed: 19384442]
52. Wang C, Zhang T, Lin W. *Chemical Reviews*. 1122011; :1084–1104. [PubMed: 22070202]
53. Evans OR, Lin W. *Accounts of Chemical Research*. 352002; :511–522. [PubMed: 12118990]
54. Zhang W, Xiong R-G. *Chemical Reviews*. 1122011; :1163–1195. [PubMed: 21939288]
55. Silva CG, Corma A, García H. *Journal of Materials Chemistry*. 202010; :3141–3156.
56. Ramaswamy P, Wong NE, Shimizu GK. *Chemical Society Reviews*. 432014; :5913–5932. [PubMed: 24733639]
57. Talin AA, Centrone A, Ford AC, Foster ME, Stavila V, Haney P, Kinney RA, Szalai V, El Gabaly F, Yoon HP. *Science*. 2013:1246738.
58. Allendorf M, Bauer C, Bhakta R, Houk R. *Chemical Society Reviews*. 382009; :1330–1352. [PubMed: 19384441]
59. Xie Z, Ma L, deKrafft KE, Jin A, Lin W. *Journal of the American Chemical Society*. 1322009; :922–923.
60. Kreno LE, Leong K, Farha OK, Allendorf M, Van Duyne RP, Hupp JT. *Chemical Reviews*. 1122012; :1105–1125. [PubMed: 22070233]
61. Cui Y, Yue Y, Qian G, Chen B. *Chemical Reviews*. 1122011; :1126–1162. [PubMed: 21688849]
62. Hu Z, Deibert BJ, Li J. *Chemical Society Reviews*. 432014; :5815–5840. [PubMed: 24577142]
63. Liu J, Chen L, Cui H, Zhang J, Zhang L, Su C-Y. *Chemical Society Reviews*. 432014; :6011–6061. [PubMed: 24871268]
64. Seo JS, Whang D, Lee H, Im Jun S, Oh J, Jeon YJ, Kim K. *Nature*. 4042000; :982–986. [PubMed: 10801124]
65. Lee J, Farha OK, Roberts J, Scheidt KA, Nguyen ST, Hupp JT. *Chemical Society Reviews*. 382009; :1450–1459. [PubMed: 19384447]
66. Ma L, Falkowski JM, Abney C, Lin W. *Nature Chemistry*. 22010; :838–846.
67. Zhao M, Ou S, Wu C-D. *Accounts of Chemical Research*. 472014; :1199–1207. [PubMed: 24499017]
68. Corma A, García H, Llabrés i Xamena F. *Chemical Reviews*. 1102010; :4606–4655. [PubMed: 20359232]
69. Kent CA, Mehl BP, Ma L, Papanikolas JM, Meyer TJ, Lin W. *Journal of the American Chemical Society*. 1322010; :12767–12769. [PubMed: 20735124]
70. Zhang T, Lin W. *Chemical Society Reviews*. 432014; :5982–5993. [PubMed: 24769551]
71. Wang J-L, Wang C, Lin W. *ACS Catalysis*. 22012; :2630–2640.
72. Liu D, Lu K, Poon C, Lin W. *Inorganic Chemistry*. 532013; :1916–1924. [PubMed: 24251853]
73. Rieter WJ, Taylor KM, An H, Lin W, Lin W. *Journal of the American Chemical Society*. 1282006; :9024–9025. [PubMed: 16834362]
74. Taylor KM, Rieter WJ, Lin W. *Journal of the American Chemical Society*. 1302008; :14358–14359. [PubMed: 18844356]
75. Della Rocca J, Liu D, Lin W. *Accounts of Chemical Research*. 442011; :957–968. [PubMed: 21648429]
76. Horcajada P, Serre C, Vallet - Regí M, Sebban M, Taulelle F, Férey G. *Angewandte Chemie*. 1182006; :6120–6124.
77. Taylor-Pashow KM, Rocca JD, Xie Z, Tran S, Lin W. *Journal of the American Chemical Society*. 1312009; :14261–14263. [PubMed: 19807179]
78. Horcajada P, Gref R, Baati T, Allan PK, Maurin G, Couvreur P, Férey G, Morris RE, Serre C. *Chemical Reviews*. 1122011; :1232–1268. [PubMed: 22168547]
79. Horcajada P, Chalati T, Serre C, Gillet B, Sebrie C, Baati T, Eubank JF, Heurtaux D, Clayette P, Kreuz C. *Nature Materials*. 92010; :172–178. [PubMed: 20010827]
80. Celli JP, Spring BQ, Rizvi I, Evans CL, Samkoe KS, Verma S, Pogue BW, Hasan T. *Chemical Reviews*. 1102010; :2795–2838. [PubMed: 20353192]
81. Ng KK, Zheng G. *Chemical Reviews*. 1152015; :11012–11042. [PubMed: 26244706]

82. Plaetzer K, Krammer B, Berlanda J, Berr F, Kiesslich T. *Lasers in Medical Science*. 242009; :259–268. [PubMed: 18247081]
83. Castano AP, Demidova TN, Hamblin MR. *Photodiagnosis and Photodynamic Therapy*. 12004; :279–293. [PubMed: 25048432]
84. Ochsner M. *Journal of Photochemistry and Photobiology B: Biology*. 391997; :1–18.
85. Yoon I, Li JZ, Shim YK. *Clinical Endoscopy*. 462013; :7. [PubMed: 23423543]
86. Benov L. *Medical Principles and Practice*. 242015; :14–28. [PubMed: 24820409]
87. Gouterman M. *The Porphyrins*. 31978;
88. Gouterman M. *Journal of Molecular Spectroscopy*. 61961; :138–163.
89. Kelly J, Snell M. *The Journal of Urology*. 1151976; :150–151. [PubMed: 1249866]
90. Hayata Y, Kato H, Konaka C, Ono J, Takizawa N. *Chest*. 811982; :269–277. [PubMed: 6276108]
91. Abrahamse H, Hamblin MR. *Biochemical Journal*. 4732016; :347–364. [PubMed: 26862179]
92. Bonnett R. *Chemical Society Reviews*. 241995; :19–33.
93. Gomer CJ. *Photochemistry and Photobiology*. 541991; :1093–1107. [PubMed: 1775531]
94. Lovell JF, Liu TW, Chen J, Zheng G. *Chemical Reviews*. 1102010; :2839–2857. [PubMed: 20104890]
95. Ballut S, Makky A, Chauvin B, Michel J-P, Kasselouri A, Maillard P, Rosilio V. *Organic & Biomolecular Chemistry*. 102012; :4485–4495. [PubMed: 22569817]
96. Hamblin MR, Newman EL. *Journal of Photochemistry and Photobiology B: Biology*. 261994; :45–56.
97. Demidova TN, Hamblin MR. *Antimicrobial Agents and Chemotherapy*. 492005; :2329–2335. [PubMed: 15917529]
98. Demidova T, Hamblin M. *International Journal of Immunopathology and Pharmacology*. 172004; :117. [PubMed: 15171812]
99. You H, Yoon H-E, Jeong P-H, Ko H, Yoon J-H, Kim Y-C. *Bioorganic & Medicinal Chemistry*. 232015; :1453–1462. [PubMed: 25753328]
100. Kaš áková S, Hofland LJ, De Bruijn HS, Ye Y, Achilefu S, van der Wansem K, van Koetsveld PM, Brugts MP, van der Lelij A-J, Sterenborg HJ. *PloS one*. 92014; :e104448. [PubMed: 25111655]
101. Goff B, Hermanto U, Rumbaugh J, Blake J, Bamberg M, Hasan T. *British Journal of Cancer*. 701994; :474–480. [PubMed: 8080733]
102. Staggers N, McCasky T, Brazelton N, Kennedy R. *Nursing Outlook*. 562008; :268–274. [PubMed: 18922283]
103. Huang Y-Y, Sharma SK, Dai T, Chung H, Yaroslavsky A, Garcia-Diaz M, Chang J, Chiang LY, Hamblin MR. *Nanotechnology Reviews*. 12012; :111–146. [PubMed: 26361572]
104. Wilson MD, Chopp M. *Lasers in Surgery and Medicine*. 221998; :74–80. [PubMed: 9484699]
105. Derycke AS, de Witte PA. *Advanced Drug Delivery Reviews*. 562004; :17–30. [PubMed: 14706443]
106. Konan YN, Gurny R, Allémann E. *Journal of Photochemistry and Photobiology B: Biology*. 662002; :89–106.
107. Nishiyama N, Morimoto Y, Jang W-D, Kataoka K. *Advanced Drug Delivery Reviews*. 612009; :327–338. [PubMed: 19385091]
108. Zhang G-D, Harada A, Nishiyama N, Jiang D-L, Koyama H, Aida T, Kataoka K. *Journal of Controlled Release*. 932003; :141–150. [PubMed: 14636720]
109. Cheng Y, Samia AC, Meyers JD, Panagopoulos I, Fei B, Burda C. *Journal of the American Chemical Society*. 1302008; :10643–10647. [PubMed: 18642918]
110. Hone DC, Walker PI, Evans-Gowing R, FitzGerald S, Beeby A, Chambrier I, Cook MJ, Russell DA. *Langmuir*. 182002; :2985–2987.
111. Kim S, Ohulchanskyy TY, Pudavar HE, Pandey RK, Prasad PN. *Journal of the American Chemical Society*. 1292007; :2669–2675. [PubMed: 17288423]
112. Ohulchanskyy TY, Roy I, Goswami LN, Chen Y, Bergey EJ, Pandey RK, Oseroff AR, Prasad PN. *Nano letters*. 72007; :2835–2842. [PubMed: 17718587]

113. Qian HS, Guo HC, Ho PCL, Mahendran R, Zhang Y. *Small*. 52009; :2285–2290. [PubMed: 19598161]
114. Lovell JF, Jin CS, Huynh E, Jin H, Kim C, Rubinstein JL, Chan WC, Cao W, Wang LV, Zheng G. *Nature Materials*. 102011; :324–332. [PubMed: 21423187]
115. Yoon HK, Lou X, Chen Y-C, Koo Lee Y-E, Yoon E, Kopelman R. *Chemistry of Materials*. 262014; :1592–1600. [PubMed: 24701030]
116. Liu K, Xing R, Zou Q, Ma G, Möhwald H, Yan X. *Angewandte Chemie International Edition*. 552016; :3036–3039. [PubMed: 26804551]
117. Zhang N, Zhao F, Zou Q, Li Y, Ma G, Yan X. *Small*. 122016; :5936–5943. [PubMed: 27622681]
118. Yang X, Fei J, Li Q, Li J. *Chemistry-A European Journal*. 222016; :6477–6481.
119. Dekrafft KE, Xie Z, Cao G, Tran S, Ma L, Zhou OZ, Lin W. *Angewandte Chemie*. 1212009; :10085–10088.
120. Boyle WS, Burk LM, Zhou OZ, Lin W. *Journal of Materials Chemistry*. 222012; :18139–18144. [PubMed: 23049169]
121. Foucault-Collet A, Gogick KA, White KA, Villette S, Pallier A, Collet G, Kieda C, Li T, Geib SJ, Rosi NL. *Proceedings of the National Academy of Sciences*. 1102013; :17199–17204.
122. He C, Lu K, Lin W. *Journal of the American Chemical Society*. 1362014; :12253–12256. [PubMed: 25136764]
123. Xu R, Wang Y, Duan X, Lu K, Micheroni D, Hu A, Lin W. *Journal of the American Chemical Society*. 1382016; :2158–2161. [PubMed: 26864385]
124. He C, Lu K, Liu D, Lin W. *Journal of the American Chemical Society*. 1362014; :5181–5184. [PubMed: 24669930]
125. Huxford RC, Boyle WS, Liu D, Lin W. *Chemical Science*. 32012; :198–204.
126. Taylor KM, Jin A, Lin W. *Angewandte Chemie*. 1202008; :7836–7839.
127. Lu K, He C, Lin W. *Journal of the American Chemical Society*. 1362014; :16712–16715. [PubMed: 25407895]
128. Lu K, He C, Lin W. *Journal of the American Chemical Society*. 1372015; :7600–7603. [PubMed: 26068094]
129. Lu K, He C, Guo N, Chan C, Ni K, Weichselbaum RR, Lin W. *Journal of the American Chemical Society*. 1382016; :12502–12510. [PubMed: 27575718]
130. Park J, Feng D, Yuan S, Zhou HC. *Angewandte Chemie*. 1272015; :440–445.
131. Liu J, Yang Y, Zhu W, Yi X, Dong Z, Xu X, Chen M, Yang K, Lu G, Jiang L. *Biomaterials*. 972016; :1–9. [PubMed: 27155362]
132. Zhang L, Lei J, Ma F, Ling P, Liu J, Ju H. *Chemical Communications*. 512015; :10831–10834. [PubMed: 26051476]
133. Park J, Jiang Q, Feng D, Zhou HC. *Angewandte Chemie International Edition*. 552016; :7188–7193. [PubMed: 27126322]
134. Park J, Jiang Q, Feng D, Mao L, Zhou H-C. *Journal of the American Chemical Society*. 1382016; :3518–3525. [PubMed: 26894555]
135. Wang W, Wang L, Li Z, Xie Z. *Chemical Communications*. 522016; :5402–5405. [PubMed: 27009757]
136. Cai H-J, Shen T-T, Zhang J, Shan C-F, Jia J-G, Li X, Liu W-S, Tang Y. *Journal of Materials Chemistry B*. 52017; :2390–2394.
137. Yang D, Yang G, Gai S, He F, An G, Dai Y, Lv R, Yang P. *Nanoscale*. 72015; :19568–19578. [PubMed: 26540558]
138. Zhang H, Li Y-H, Chen Y, Wang M-M, Wang X-S, Yin X-B. *Scientific Reports*. 72017;
139. He L, Brasino M, Mao C, Cho S, Park W, Goodwin AP, Cha JN. *Small*. 2017
140. Zheng X, Wang L, Pei Q, He S, Liu S, Xie Z. *Chemistry of Materials*. 292017; :2374–2381.
141. Liu J, Zhang L, Lei J, Shen H, Ju H. *ACS Applied Materials & Interfaces*. 92017; :2150–2158. [PubMed: 28033467]
142. B žek D, Zelenka J, Ulbrich P, Ruml T, Krizova I, Lang J, Kubat P, Demel J, Kirakci K, Lang K. *Journal of Materials Chemistry B*. 52017; :1815–1821.

143. Chen X, Zhang M, Li S, Li L, Zhang L, Wang T, Yu M, Mou Z, Wang C. *Journal of Materials Chemistry B*. 52017; :1772–1778.
144. Fang L, Wang W, Liu Y, Chen L, Xie Z. *Dalton Transactions*. 2017
145. Fu G, Liu W, Feng S, Yue X. *Chemical Communications*. 482012; :11567–11569. [PubMed: 23090583]
146. Jing L, Liang X, Deng Z, Feng S, Li X, Huang M, Li C, Dai Z. *Biomaterials*. 352014; :5814–5821. [PubMed: 24746962]
147. Su YY, Teng Z, Yao H, Wang SJ, Tian Y, Zhang YL, Liu WF, Tian W, Zheng LJ, Lu N. *ACS Applied Materials & Interfaces*. 82016; :17038–17046. [PubMed: 27065014]
148. Tian Z, Yao X, Ma K, Niu X, Grothe J, Xu Q, Liu L, Kaskel S, Zhu Y. *ACS Omega*. 22017; : 1249–1258. [PubMed: 30023630]
149. Wang D, Guo Z, Zhou J, Chen J, Zhao G, Chen R, He M, Liu Z, Wang H, Chen Q. *Small*. 112015; :5956–5967. [PubMed: 26437078]
150. Wang D, Zhou J, Chen R, Shi R, Zhao G, Xia G, Li R, Liu Z, Tian J, Wang H. *Biomaterials*. 1002016; :27–40. [PubMed: 27240160]
151. Wang S, Shang L, Li L, Yu Y, Chi C, Wang K, Zhang J, Shi R, Shen H, Waterhouse GI. *Advanced Materials*. 282016; :8379–8387. [PubMed: 27461987]
152. Yang X, Li L, He D, Hai L, Tang J, Li H, He X, Wang K. *Journal of Materials Chemistry B*. 2017
153. Yang Y, Chao Y, Liu J, Dong Z, He W, Zhang R, Yang K, Chen M, Liu Z. *NPG Asia Materials*. 92017; :e344.
154. Yang Y, Liu J, Liang C, Feng L, Fu T, Dong Z, Chao Y, Li Y, Lu G, Chen M. *ACS Nano*. 102016; :2774–2781. [PubMed: 26799993]
155. Morris W, Briley WE, Auyeung E, Cabezas MD, Mirkin CA. *Journal of the American Chemical Society*. 1362014; :7261–7264. [PubMed: 24818877]
156. Xiao B, Wheatley PS, Zhao X, Fletcher AJ, Fox S, Rossi AG, Megson IL, Bordiga S, Regli L, Thomas KM. *Journal of the American Chemical Society*. 1292007; :1203–1209. [PubMed: 17263402]
157. McKinlay AC, Xiao B, Wragg DS, Wheatley PS, Megson IL, Morris RE. *Journal of the American Chemical Society*. 1302008; :10440–10444. [PubMed: 18627150]
158. McKinlay A, Eubank J, Wuttke S, Xiao B, Wheatley P, Bazin P, Lavalley J-C, Daturi M, Vimont A, De Weireld G. *Chemistry of Materials*. 252013; :1592–1599.
159. Lan G, Ni K, Xu R, Lu K, Lin Z, Chan C, Lin W. *Angewandte Chemie International Edition*. 2017; doi: 10.1002/anie.201704828
160. Dai R, Peng F, Ji P, Lu K, Wang C, Sun J, Lin W. *Inorganic Chemistry*. 2017
161. Novak K. *Nature Reviews Cancer*. 32003; :887–887.
162. Aioub M, El-Sayed MA. *Journal of the American Chemical Society*. 1382016; :1258–1264. [PubMed: 26746480]
163. Bardhan R, Chen W, Perez - Torres C, Bartels M, Huschka RM, Zhao LL, Morosan E, Pautler RG, Joshi A, Halas NJ. *Advanced Functional Materials*. 192009; :3901–3909.
164. Zhang Z, Wang L, Wang J, Jiang X, Li X, Hu Z, Ji Y, Wu X, Chen C. *Advanced Materials*. 242012; :1418–1423. [PubMed: 22318874]
165. Wang S, Huang P, Nie L, Xing R, Liu D, Wang Z, Lin J, Chen S, Niu G, Lu G. *Advanced Materials*. 252013; :3055–3061. [PubMed: 23404693]
166. Xia Y, Li W, Cogley CM, Chen J, Xia X, Zhang Q, Yang M, Cho EC, Brown PK. *Accounts of Chemical Research*. 442011; :914–924. [PubMed: 21528889]
167. Chen Y-W, Su Y-L, Hu S-H, Chen S-Y. *Advanced Drug Delivery Reviews*. 1052016; :190–204. [PubMed: 27262922]
168. Song J, Wang F, Yang X, Ning B, Harp MG, Culp SH, Hu S, Huang P, Nie L, Chen J. *Journal of the American Chemical Society*. 1382016; :7005–7015. [PubMed: 27193381]
169. Ryu TK, Baek SW, Kang RH, Choi SW. *Advanced Functional Materials*. 262016; :6428–6436.
170. Shen S, Wang S, Zheng R, Zhu X, Jiang X, Fu D, Yang W. *Biomaterials*. 392015; :67–74. [PubMed: 25477173]

171. Tang S, Chen M, Zheng N. *Small*. 102014; :3139–3144. [PubMed: 24729448]
172. Tian Q, Hu J, Zhu Y, Zou R, Chen Z, Yang S, Li R, Su Q, Han Y, Liu X. *Journal of the American Chemical Society*. 1352013; :8571–8577. [PubMed: 23687972]
173. Zhang C, Bu W, Ni D, Zuo C, Cheng C, Li Q, Zhang L, Wang Z, Shi J. *Journal of the American Chemical Society*. 1382016; :8156–8164. [PubMed: 27264421]
174. Zha Z, Yue X, Ren Q, Dai Z. *Advanced Materials*. 252013; :777–782. [PubMed: 23143782]
175. Song X, Gong H, Yin S, Cheng L, Wang C, Li Z, Li Y, Wang X, Liu G, Liu Z. *Advanced Functional Materials*. 242014; :1194–1201.
176. Lyu Y, Fang Y, Miao Q, Zhen X, Ding D, Pu K. *ACS Nano*. 102016; :4472–4481. [PubMed: 26959505]
177. U. Food, D. Administration. 2010
178. Uemura T, Ohba M, Kitagawa S. *Inorganic Chemistry*. 432004; :7339–7345. [PubMed: 15530083]
179. Cheng Y, Doane TL, Chuang CH, Ziady A, Burda C. *Small*. 102014; :1799–1804. [PubMed: 24515950]

Highlights

1. Systematic study of four generations of photosensitizers for photodynamic therapy.
2. The application of nanoscale metal-organic frameworks as nanophotosensitizers in photodynamic therapy.
3. The application of nanoscale metal-organic frameworks in photothermal therapy.

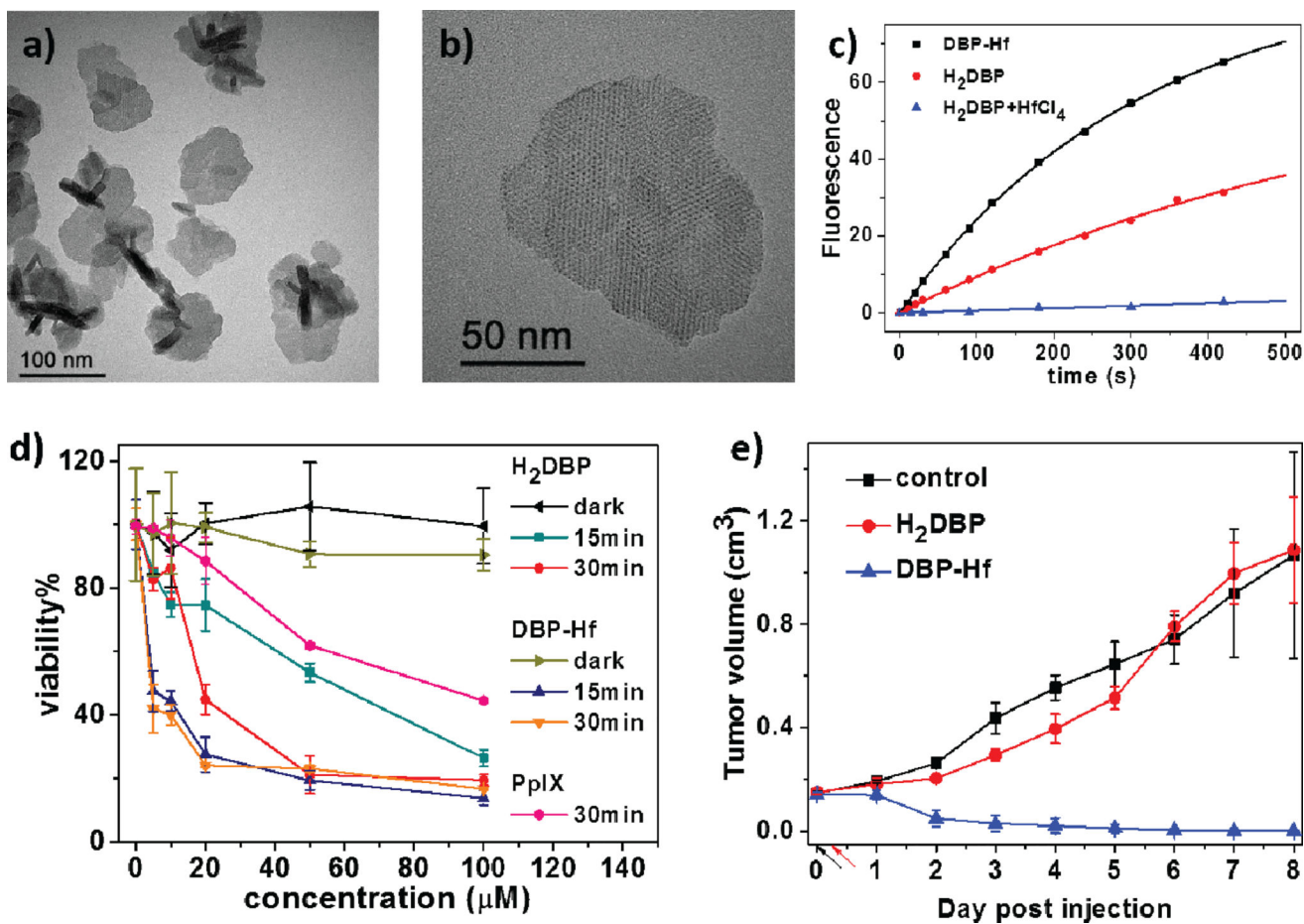


Fig. 1.

(a) TEM image and (b) high-resolution TEM image of DBP-Hf. (c) Singlet oxygen generation of DBP-Hf, H₂DBP, and H₂DBP+HfCl₄ with SOSG assay. (d) *In vitro* PDT cytotoxicity of DBP-Hf and H₂DBP. (e) *In vivo* tumor growth inhibition curve of DBP-Hf and H₂DBP. Black and red arrows refer to the time of injection and light irradiation, respectively. Reprinted with permission from ref. [127]. Copyright 2014 American Chemical Society.

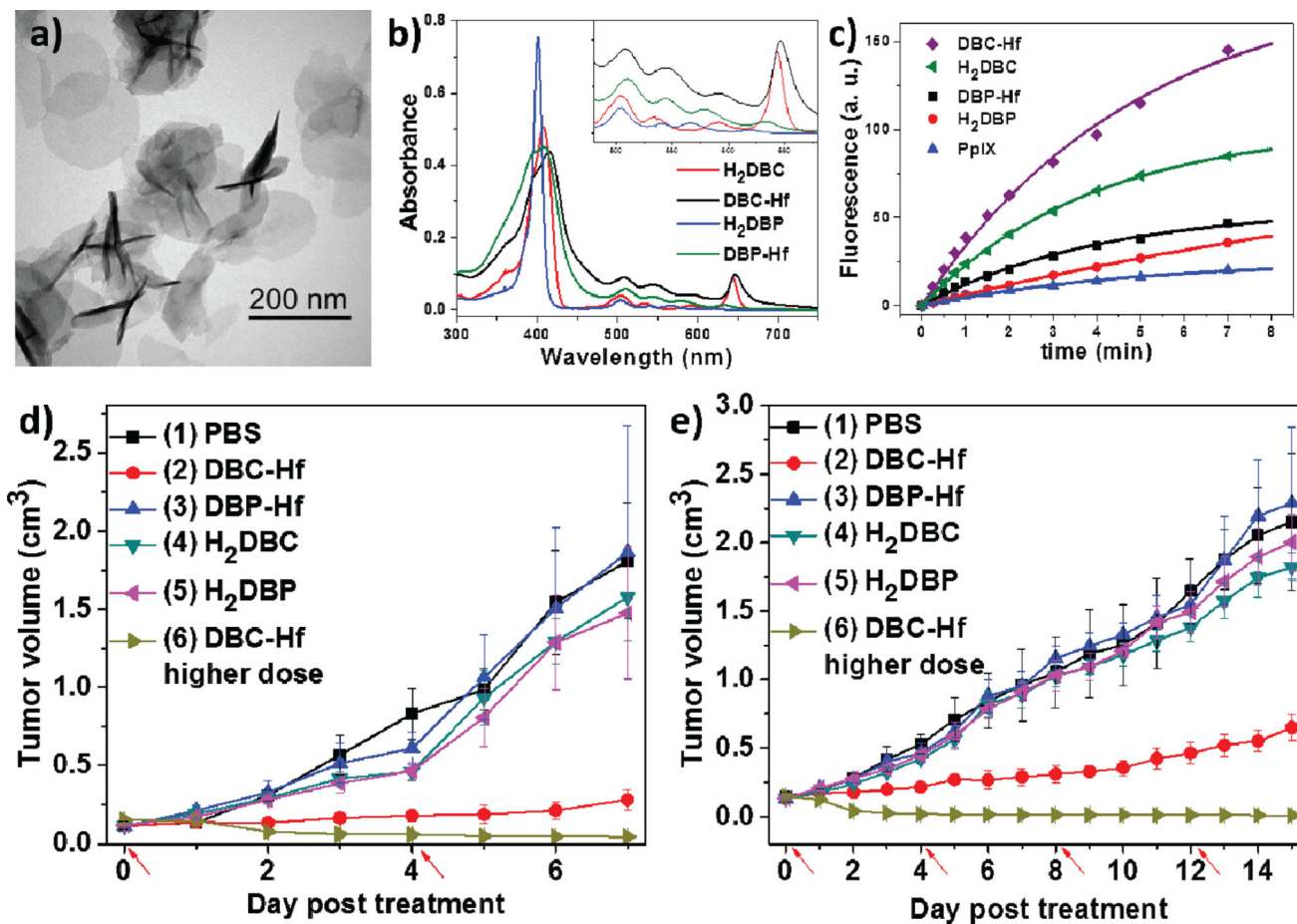


Fig. 2. (a) TEM image of DBC-Hf. Uv-vis spectra (b) and singlet oxygen generation (c) of DBC-Hf, DBP-Hf, H₂DBC and H₂DBP. Tumor growth inhibition curves after PDT treatment in CT26 (e) and HT29 (f) models. Red arrows refer to the time of light irradiation. Reprinted with permission from ref. [128]. Copyright 2015 American Chemical Society.

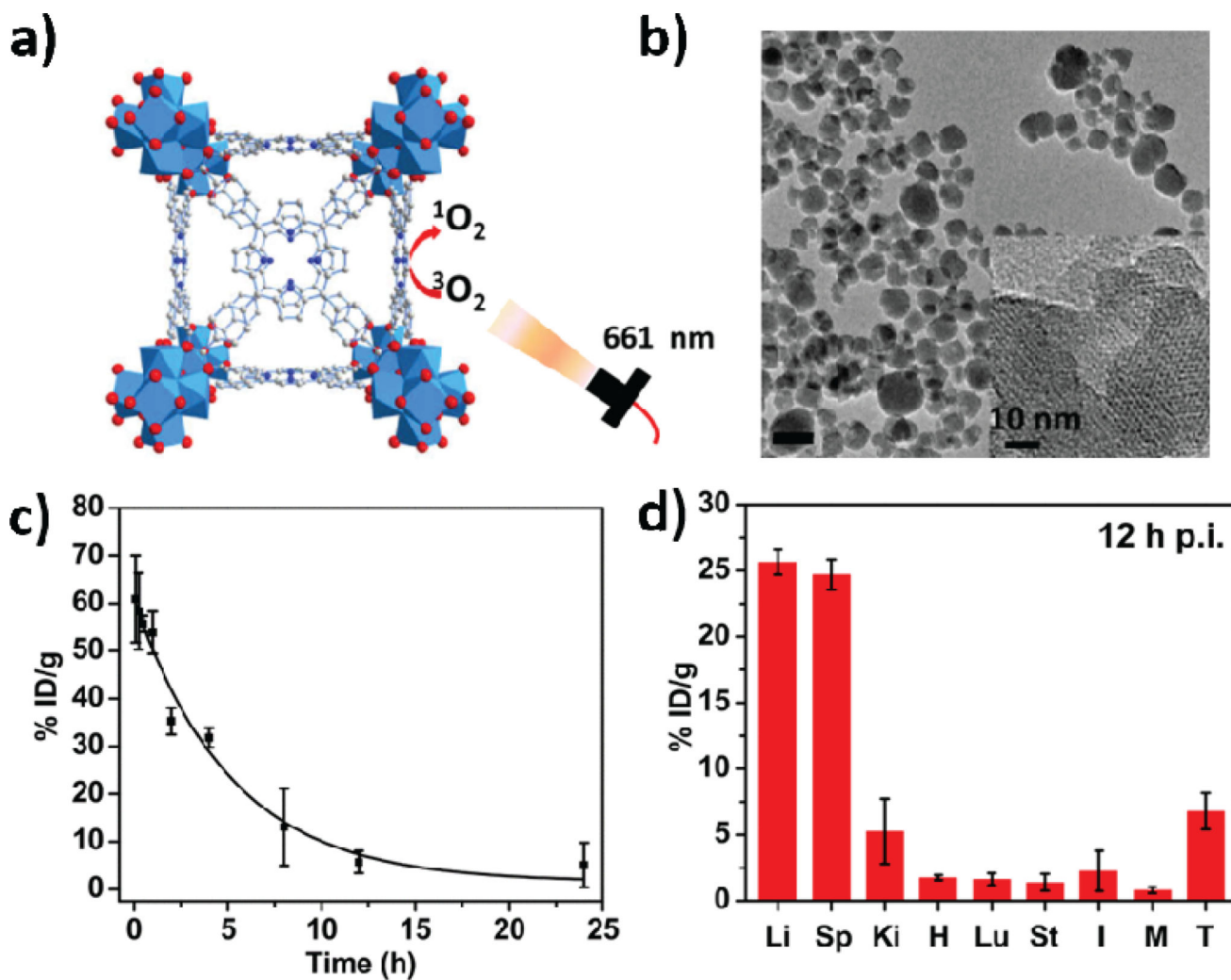


Fig. 3. (a) Schematic presentation of singlet oxygen generation by Hf-TCPP-PEG. (b) TEM image of Hf-TCPP. (c) Blood circulation of Hf-TCPP-PEG in healthy mice. (d) Biodistribution of Hf-TCPP-PEG in 4T1 tumor-bearing mice at 12 h post injection. Reprinted with permission from ref. [131]. Copyright 2016 Elsevier Ltd.

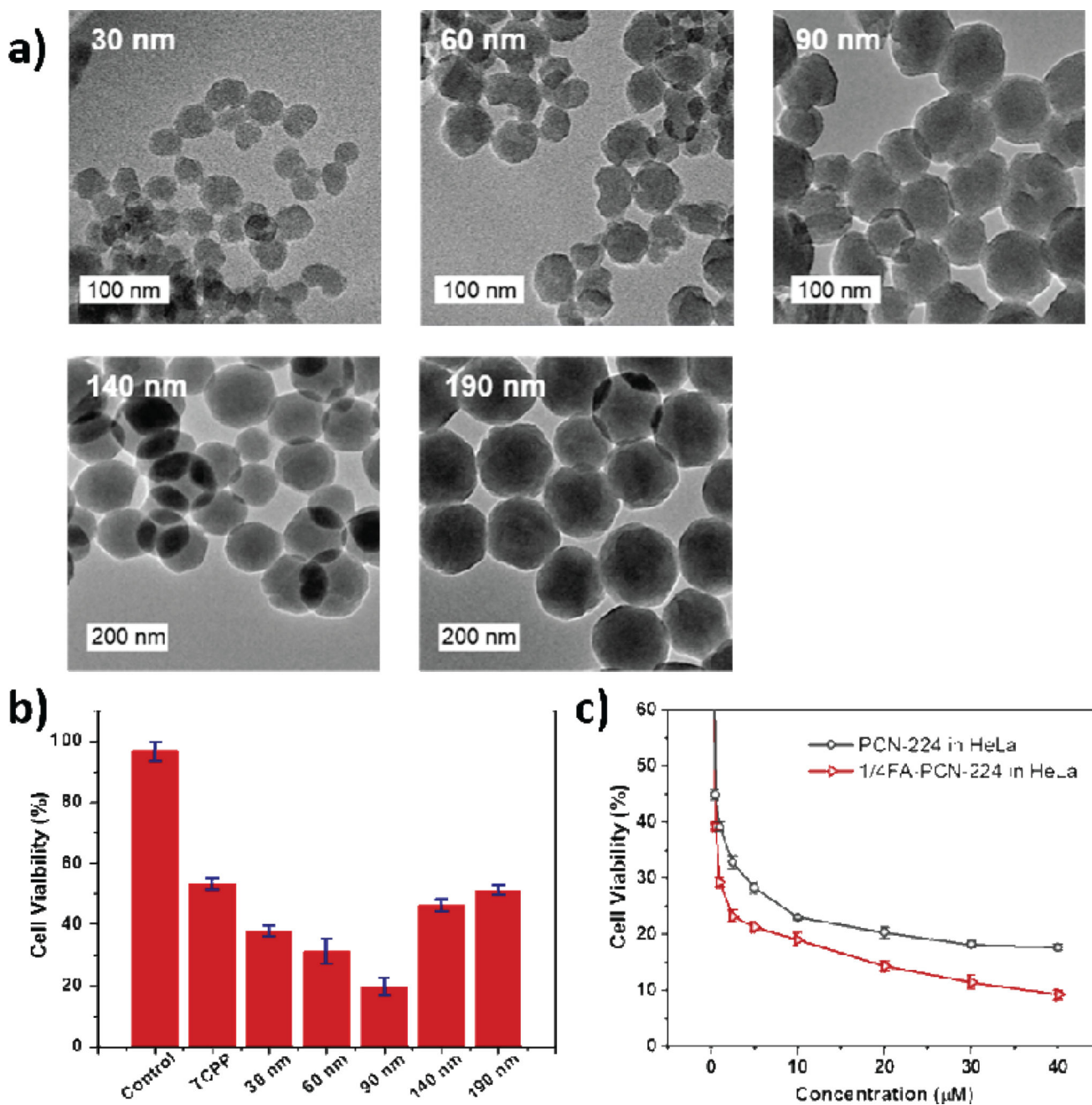


Fig. 4.

(a) TEM images of PCN-224 with different sizes. (b) *In vitro* PDT cytotoxicity efficacy of different sized PCN-224. (c) *In vitro* PDT cytotoxicity efficacy of pristine PCN-224 and 1/4FA-PCN-224 in HeLa cells. Reprinted with permission from ref. [134]. Copyright 2016 American Chemical Society.

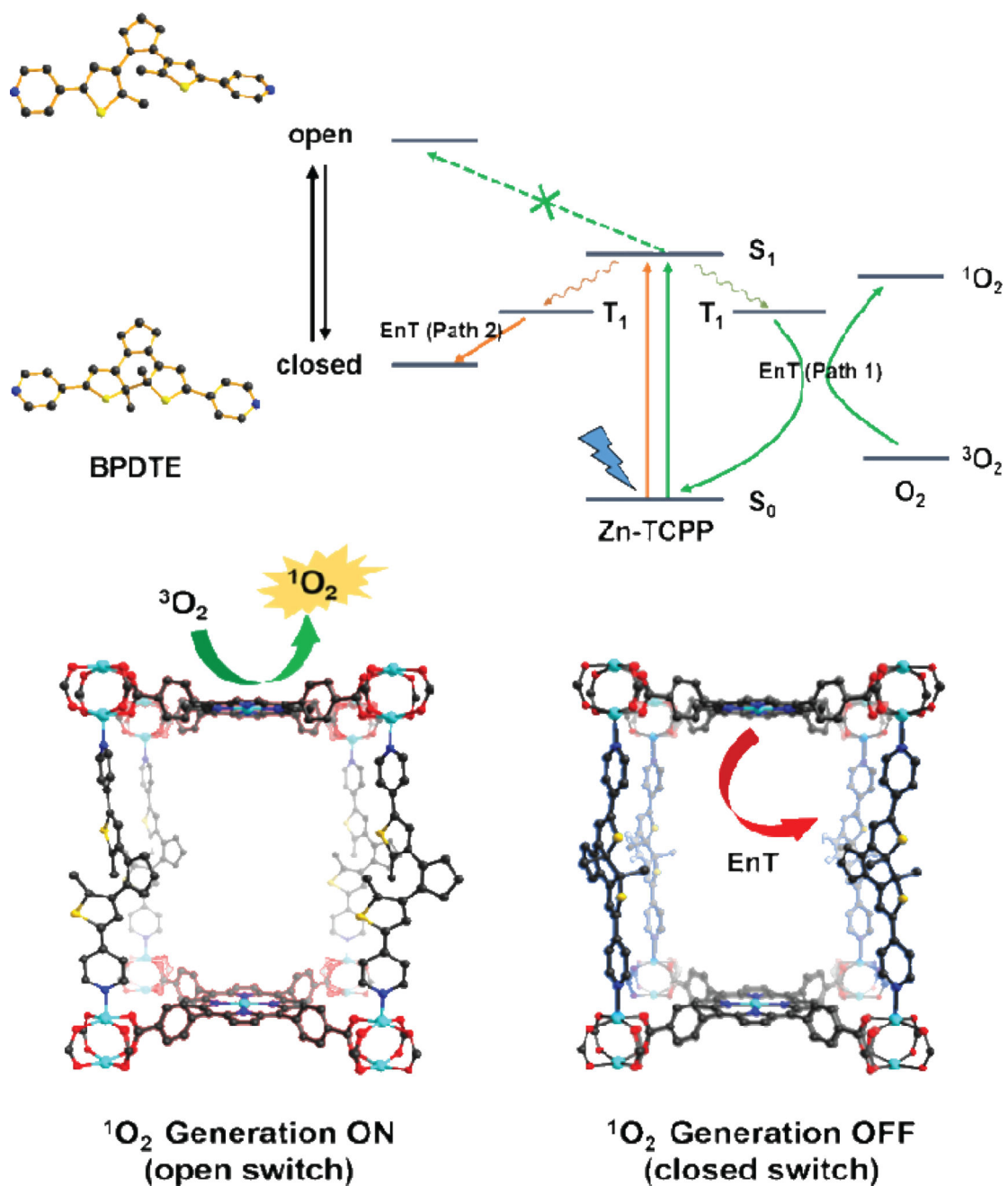


Fig. 5. Proposed mechanism of energy transfer in SO-PCN and illustration of switching operation in SO-PCN. Reprinted with permission from ref. [130]. Copyright 2015 Wiley.

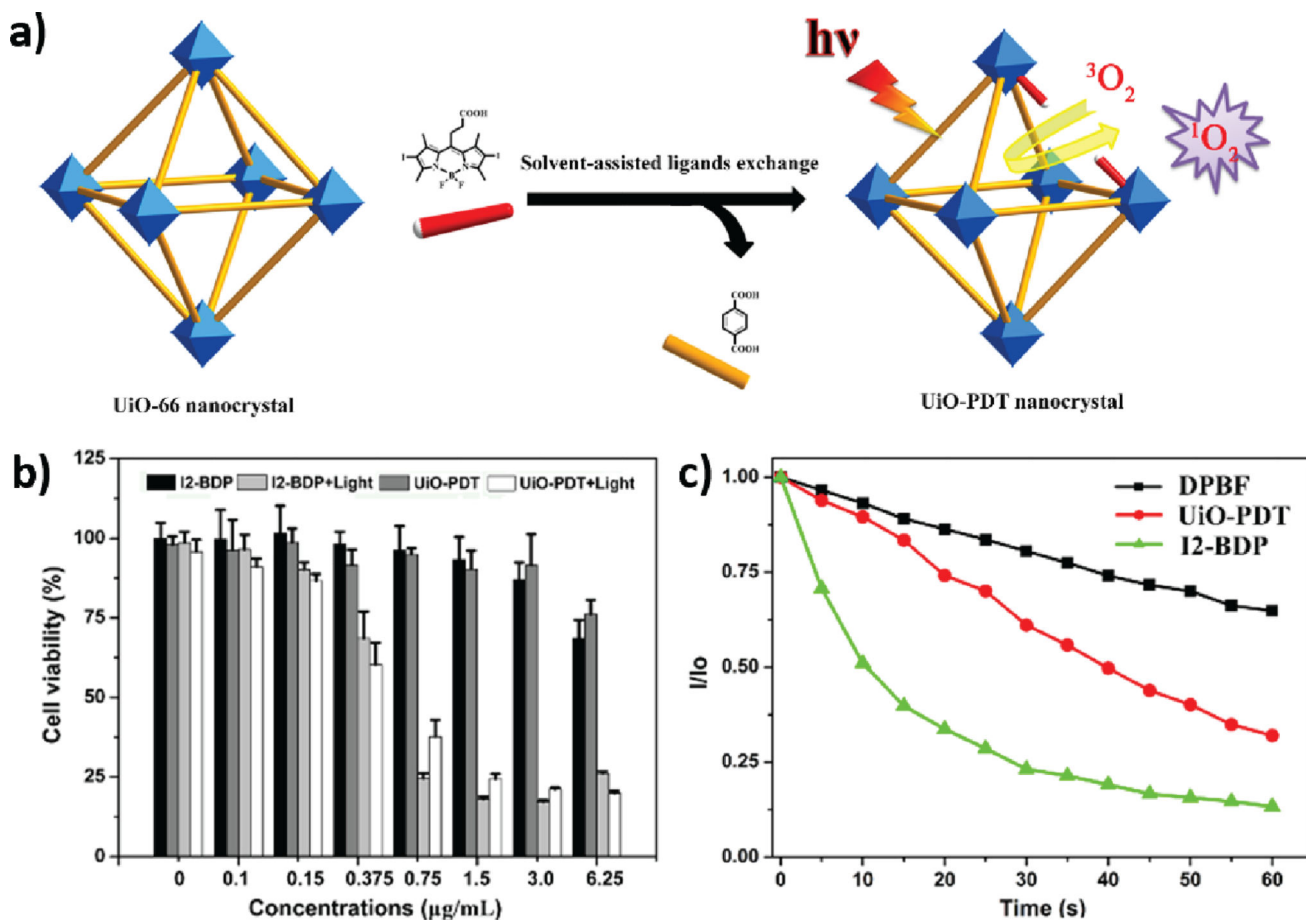


Fig. 6. (a) Proposed mechanism of synthesis of UiO-PDT. (b) Singlet oxygen generation of UiO-PDT and I2-BDP with DPBF assay. (c) *In vitro* PDT cytotoxicity efficacy of UiO-PDT and I2-BDP in B16F10 cells. Reprinted with permission of ref. [135]. Copyright 2016 Royal Society of Chemistry.

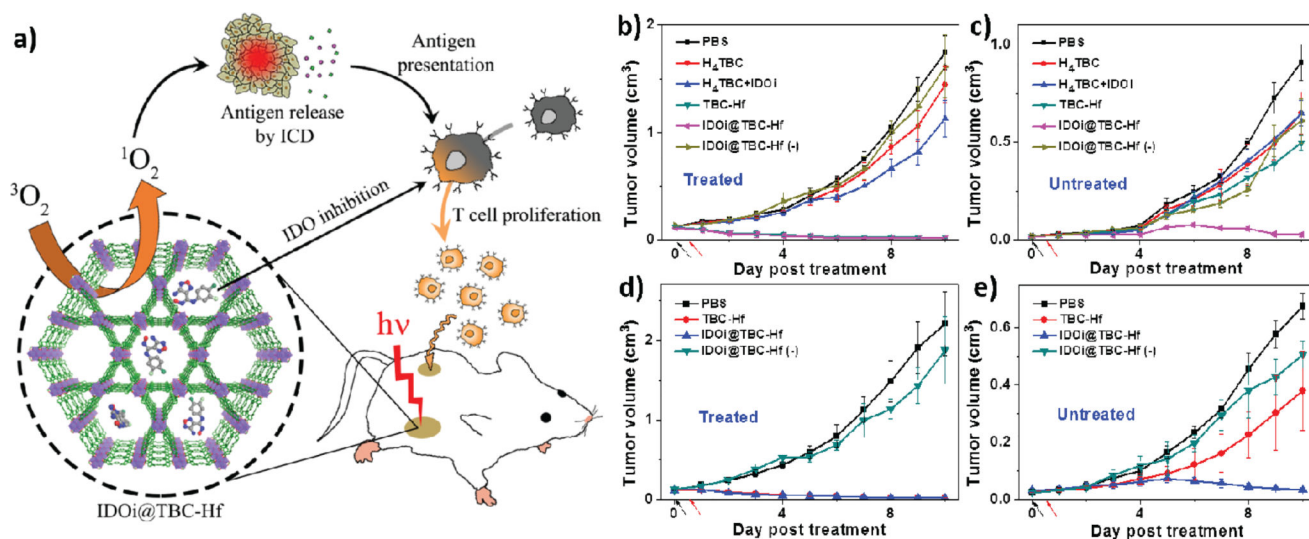


Fig. 7. (a) Schematic presentation of combined PDT and immunotherapy by IDOi@TBC-Hf. Tumor inhibition curves for treated (b, d) and untreated (c, e) tumors of CT26 (b, c) or MC38 (d, e) models after PDT treatment. Black and red arrows refer to the time of injection and light irradiation, respectively. Reprinted with permission from ref. [129]. Copyright 2016 American Chemical Society.

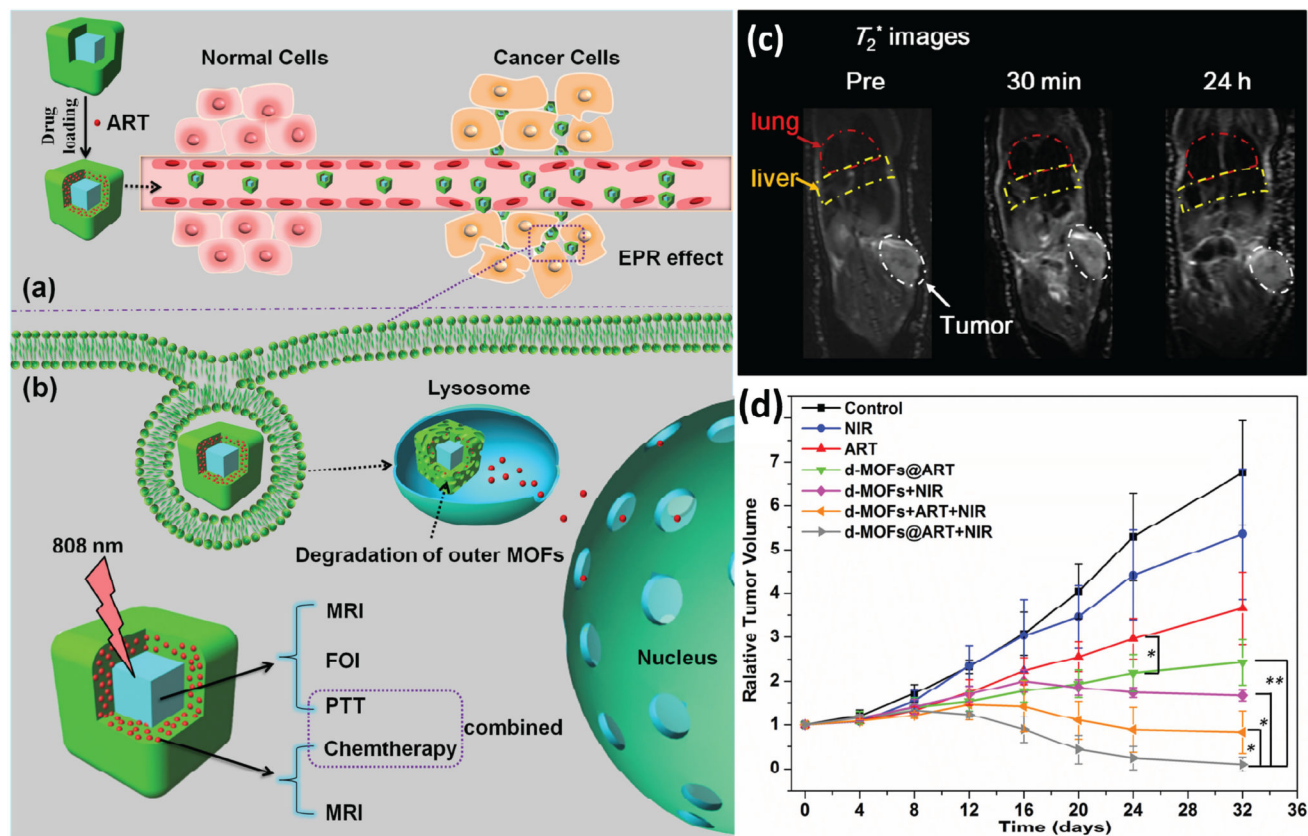


Fig. 8. (a) Schematic figures of drug loading and EPR targeting strategy. (b) pH-responsive outer MOFs for drug release and dual-modal optical- and MRI-guided cancer therapy *in vitro* and *in vivo*. (c) MRI T_2^* images of lung, liver and tumor before, 30 min and 24 h after intravenous injection of d-MOFs. (d) Tumor growth curves after treatments. Reprinted with permission of ref. [150]. Copyright 2016 Elsevier Ltd.

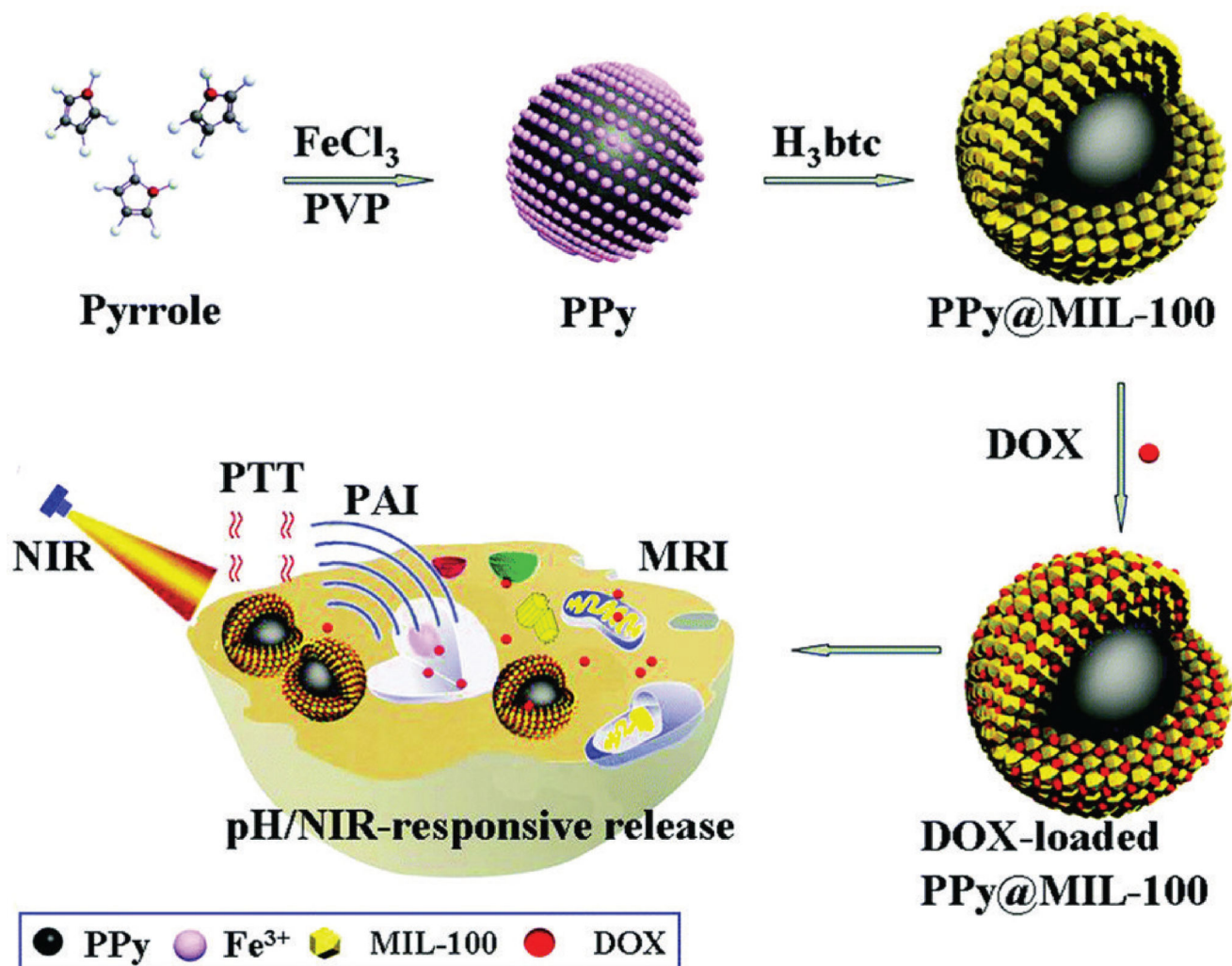


Fig. 9. Schematic figure of the synthetic strategy for PPy@MIL-100(Fe) as pH/NIR-responsive drug carriers for MRI/PAI dual-modality imaging and PTT/chemo synergistic therapy. Reprinted with permission of ref. [143]. Copyright 2016 Royal Society of Chemistry.

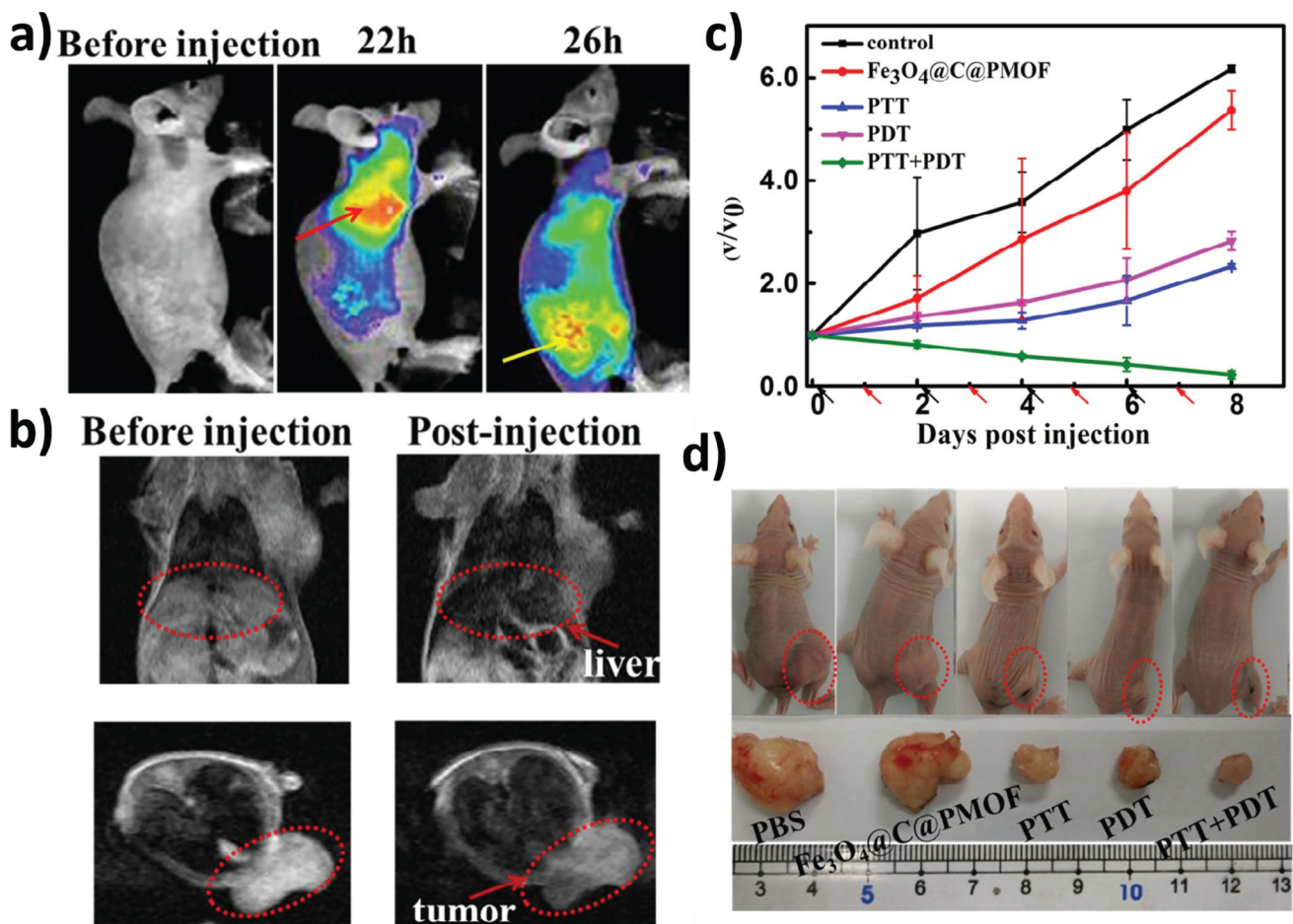


Fig. 10.

(a) Fluorescent imaging of tumor-bearing mice before and after intravenous injection of $\text{Fe}_3\text{O}_4@\text{C}@PMOF$. The red arrow points to liver region and the yellow arrow points to tumor region. (b) MRI T_2 images of tumor-bearing mice. (c) Tumor growth curves after treatment. V_0 and V refer to tumor volumes before and after PTT and/or PDT treatment with $\text{Fe}_3\text{O}_4@\text{C}@PMOF$. Black and red arrows refer to injection and irradiation time points, respectively. (d) Representative optical images of tumor-bearing mice after treatments. Reprinted with permission of ref. [138]. Copyright 2017 Nature Publishing Group.

Table 1

Summary of nMOFs for PDT applications

nMOFs	PSs: type; position; loading	Cell lines & PSs/nMOFs Concentration	Irradiation: wavelength; power; time	Anti-cancer Efficacy	Ref.
DBP-Hf Nanoplate ~100×10 nm ²	Porphyrin (DBP); Ligands; 77 wt%	SQ20B cells <i>In vitro</i> : 20 μM DBP <i>In vivo</i> : 3.5 mg DBP/kg	640 nm 100 mW/cm ² <i>In vitro</i> : 15 min <i>In vivo</i> : 30 min	<i>In vitro</i> : ~20% cell viability <i>In vivo</i> : Tumor decreased from ~150 to ~3 mm ³	[127]
DBC-Hf Nanoplate ~150×5 nm ²	Cholrin (DBC); Ligands; 64 wt%	CT26 & HT29 cells <i>In vitro</i> : 20 μM DBC <i>In vivo</i> : 1 mg DBC-Hf/kg	650 nm 100 mW/cm ² <i>In vitro</i> : 15 min <i>In vivo</i> : 15 min	<i>In vitro</i> : ~20% cell viability <i>In vivo</i> : Tumor decreased from ~2.5 to ~0.5 g	[128]
Zn-MOF Bulk	Porphyrin (TCPP); Ligands;				[130]
TMPyP@H KUST-1 ~100 nm	Porphyrin (TMPyP); Encapsulated in HKUST-1; 32.8 wt%	HeLa cells <i>In vitro</i> : 3.5 μM TMPyP	660 nm 100 mW/cm ² <i>In vitro</i> : 15 min	<i>In vitro</i> : ~30% cell viability	[132]
IDOi@TBC-Hf Nanorice ~75×45 nm	Cholrin (TBC); Ligands; TBC: 62 wt% IDOi: 4.7%	CT26 & MC38 cells <i>In vitro</i> : 20 μM TBC <i>In vivo</i> : 20 μmol TBC/kg 1.5 mg IDOi/kg	650 nm 100 mW/cm ² <i>In vitro</i> : 15 min <i>In vivo</i> : 15 min	<i>In vitro</i> : ~15% cell viability, immunogenic cell death <i>In vivo</i> : Abscopal effect, both treated and untreated tumor regressed	[129]
Hf-TCPP-P EG ~130 nm	Porphyrin (TCPP); Ligands; 55 wt%	4T1 cells <i>In vitro</i> : 80 mg TBC/L <i>In vivo</i> : 0.5 mg TCPP/mouse	661 nm 5 mW/cm ² <i>In vitro</i> : 15 min <i>In vivo</i> : 60 min X-ray: 6Gy	<i>In vitro</i> : ~20% cell viability, <i>In vivo</i> : Tumor grew slowly	[131]
PCN-224 ~90 nm	Porphyrin (TCPP); Ligands;	HeLa cells <i>In vitro</i> : 20 μM TCPP	420 or 630 nm 100 mW/cm ² <i>In vitro</i> : 30 min	<i>In vitro</i> : ~20% cell viability	[134]
TCPP/BCD TE@UiO-66 ~70 nm	Porphyrin (TCPP); Attached to SBUs;	B16 melanoma cells <i>In vitro</i> : 20 μM TCPP	420 nm 100 mW/cm ² <i>In vitro</i> : 30 min	<i>In vitro</i> : ~30% cell viability	[133]
UiO-PDT ~70 nm	BODIPY (I2-BDP); Replaced the ligands; 31.4 wt%	B16F10, CT26, and C26 Cells <i>In vitro</i> : 6.25 μg TCPP	80mW/cm ² <i>In vitro</i> : 10 min	<i>In vitro</i> : <20% cell viability for B16F10 and CT26 cells, <10% cell viability for C26 cells	[135]
IDOi@TBC-Hf Nanorice ~75×45 nm	Cholrin (TBC); Ligands; TBC: 62 wt% IDOi: 4.7%	CT26 & MC38 cells <i>In vitro</i> : 20 μM TBC <i>In vivo</i> : 20 μmol TBC/kg 1.5 mg IDOi/kg	650 nm 100 mW/cm ² <i>In vitro</i> : 15 min <i>In vivo</i> : 15 min	<i>In vitro</i> : ~15% cell viability, immunogenic cell death <i>In vivo</i> : Abscopal effect, both treated and untreated tumor shrank	[129]
UiO-AM@POP ~176 nm	Porphyrin (H ₂ P); In POP; ~8%	HepG2 and HeLa cells <i>In vitro</i> : 25 μg/mL	450 nm 45 mW/cm ² <i>In vitro</i> : 15 min	<i>In vitro</i> : ~15% cell viability	[140]
UCNPs@P CN-224 ~52 nm	Porphyrin (TCPP); Ligands;	MDA-MB-468 cells <i>In vitro</i> : 100 μg/mL	980 nm 15.9 W/cm ² <i>In vitro</i> : 20 min	<i>In vitro</i> : ~20% cell viability	[139]
Ce6-Peptide @MIL-101 ~95 nm	Chlorin (Ce6); Encapsulated in MIL-101; 3.2 wt% 3.3	HeLa cells <i>In vitro</i> : 1.6 μM Ce6 equiv	660 nm 200 mW/cm ² <i>In vitro</i> : 5 min	<i>In vitro</i> : <10% cell viability	[141]
PCN-222 Nanorice 50–70 nm	Porphyrin (TCPP); Ligands;	HeLa cells <i>In vitro</i> : 4 μM TCPP	>600 nm 50 mW/cm ² <i>In vitro</i> : 15 min	<i>In vitro</i> : <5% cell viability	[142]

nMOFs	PSs: type; position; loading	Cell lines & PSS/nMOFs Concentration	Irradiation: wavelength; power; time	Anti-cancer Efficacy	Ref.
UCNPs/MB @ZIF-8@cat talase ~500 nm	Methylene blue (MB); Encapsulated in ZIF-8; 1.97 wt%	PL 45 Cells <i>In vitro</i> : 8 µg MB/mL	980 nm 1 W/cm ² <i>In vitro</i> : 5 min	<i>In vitro</i> : 40% cell viability	[136]

Table 2

nMOFs for various photothermal cancer treatments.

Composites	Functionality	Cell lines	Anti-cancer Efficacy	Ref.
<u>nMOF-enabled PTT</u>				
Fe ^{III} ₄ [Fe ^{II} (CN) ₆] ₃ ·nH ₂ O (PB)	PTT	Hela	<i>In vitro</i> : less than 10% cell viability after treated with 16 µg/mL particles and 1200 J/cm ² laser	[145]
PB@mIL-100(Fe) with artemisinin loaded	PTT, pH-responsivechemotherapy MRI, optical imaging,	Hela	<i>In vitro</i> : 20% cell viability after treated with 100 µg/mL particles and 600 J/cm ² laser; <i>In vivo</i> : Tumors (200 mm ³) partially eradicated treated with 25 mg/kg particles and 600 J/cm ² laser	[150]
Mn ₃ [Co(CN) ₆] ₂ @SiO ₂ @Ag with DOX loaded	Optical imaging, chemotherapy, PTT, MRI	A549, HeLa, HepG2	<i>In vitro</i> : 16.92% cell viability after treated with 100 µg/mL particles and 1200 J/cm ² laser	[149]
PB@mSiO ₂ -PEG with DOX loaded	PTT, MRI, NIR & pH-responsive chemotherapy,	MCF-7	<i>In vitro</i> : 25% cell viability after treated with 1000 µg/mL particles and 0.9 W/cm ² laser for 7 mins; <i>In vivo</i> : Tumors (100 mm ³) partially regressed treated with 25 mg/kg particles and 540 J/cm ² laser	[147]
PB@Au	PTT, CT, PAI	HT-29	<i>In vitro</i> : less than 10% cell viability after treated with 100 µg/mL particles and 900 J/cm ² laser; <i>In vivo</i> : Tumors (100 mm ³) complete eradicated without recurrence treated with 500 mg/kg particles and 900 J/cm ² laser	[146]
<u>nMOF-combined PTT</u>				
ZIF-8@ graphene dots with DOX loaded	PTT, NIR & pH-responsive chemotherapy	4T1	<i>In vitro</i> : 18% cell viability after treated with 100 µg/mL particles and 450 J/cm ² laser	[148]
Pd@Au@ZIF-8 with DOX loaded	PTT, NIR & pH-responsive chemotherapy	SMMC-7721	<i>In vitro</i> : 11% cell viability after treated with 80 µg/mL particles and 1260 J/cm ² laser	[152]
Au nanorod@ZIF-8	PTT	MCF-7	<i>In vitro</i> : 18.7% cell viability after treated with 20 µg/mL particles and 600 J/cm ² laser	[144]
Polypyrrole@mIL-100(Fe) with DOX-loaded	MRI, PAI, PTT, chemotherapy	HepG2	<i>In vitro</i> : 10% cell viability after treated with 100 µg/mL particles and 600 J/cm ² laser	[143]
<u>nMOFs for PDT + PTT</u>				
Fe ₃ O ₄ /ZIF-8-Au ₂₅	MRI, PDT, PTT	L929, HeLa	<i>In vitro</i> : 15% cell viability after treated with 500 µg/mL particles and 300 J/cm ² laser; <i>In vivo</i> : Tumors (100 mm ³) were suppressed with 300 J/cm ² laser	[137]
Fe ₃ O ₄ @C@ Porphyrin	Fluorescence, MRI, PTT, PDT	MCF-7	<i>In vitro</i> : 35% cell viability after treated with 400 µg/mL particles, 180 J/cm ² laser for PDT and 600 J/cm ² laser for PTT; <i>In vivo</i> : tumors (200 mm ³) significantly regressed after treated with 10 mg/kg particles, 180 J/cm ² laser for PDT and 600 J/cm ² laser for PTT	[138]